DEPARTMENT OF PHYSICS
Institute for Beam Physics and Technology

# Stability Improvements at FLUTE
## (Verbesserung der Stabilität von FLUTE)

Master thesis
of

Marvin-Dennis Noll

at the Institute for Beam Physics and Technology

| | |
|---|---|
| Reviewer: | Prof. Dr.-Ing. John Jelonnek (IHM) |
| Second Reviewer: | Prof. Dr. Anke-Susanne Müller (IBPT) |
| Advisor: | Dr. Nigel Smale (IBPT) |

15.11.2020 – 01.07.2021

# Erklärung zur Selbstständigkeit

Ich versichere wahrheitsgemäß, die Arbeit selbstständig angefertigt, alle benutzten Hilfsmittel vollständig und genau angegeben und alles kenntlich gemacht zu haben, was aus Arbeiten anderer unverändert oder mit Abänderungen entnommen wurde und dass ich die Satzung des KIT zur Sicherung guter wissenschaftlicher Praxis in der gültigen Fassung vom 24.05.2018 beachtet habe.

Karlsruhe, den 01.07.2021, _____

Marvin-Dennis Noll

Als Prüfungsexemplar genehmigt von

Karlsruhe, den 01.07.2021, _____

Prof. Dr.-Ing. John Jelonnek (IHM)

# Contents


**1 Introduction** **3**

**2 Theoretical Framework** **5**
2.1 Linear Accelerators . . . 5
2.1.1 Some Beam Diagnostic Devices . . . 5
2.2 Signal Analysis . . . 5
2.2.1 Auto correlation and Cross correlation . . . 5
2.2.2 Estimating the Spectrum of a Stochastic Process . . . 6
2.3 Feedback Control Systems . . . 8

**3 Current and Needed Stability of the Electron Gun** **9**

**4 Interfacing FLUTE** **11**
4.1 Inputs . . . 11
4.1.1 Accessing EPICS channels in Python with PyEpics . . . 11
4.1.2 Properties of the Available Process Variables . . . 12
4.2 Output: Controllable RF Attenuator . . . 15
4.2.1 Defining Requirements . . . 15
4.2.2 Evaluation of the ZX73-2500-S+ Controllable RF Attenuator . . . 15
4.2.2.1 Common Measurement Setup . . . 17
4.2.2.2 Relation between Control Voltage and Attenuation . . . 18
4.2.2.3 Influence of Supply Voltage Noise on Attenuation . . . 22
4.2.2.4 Influence of RF Frequency on Attenuation . . . 24
4.2.2.5 Influence of Case Temperature Variations on Attenuation . 25
4.2.2.6 $V_{control}$ Frequency response . . . 28
4.2.2.7 Combined Maximum Error of the Attenuation and Conclusion 29

**5 Controller Design and Evaluation** **31**
5.1 Architecture . . . 31
5.2 Inputs and Outputs . . . 32
5.2.1 Input . . . 32
5.2.2 Output . . . 32
5.3 Plant Identification . . . 32
5.3.1 Principle . . . 32
5.3.2 Identifying the system response of the FLUTE LLRF . . . 33
5.4 Controller design . . . 35
5.5 Software Design . . . 36
5.6 Control Parameter Tuning and Tests . . . 36
5.7 Results . . . 37

**6 Summary and Outlook** **41**

**Appendix** **43**
A Lab Test and Measurement Equipment . . . . . 43

# List of Figures

4.1 Comparing the quantization noise of three process variables . . . . . 13
4.2 Histogram of the sample time intervals $\Delta$ of the plots in Figure 4.1 . . . . . 14
4.3 Attenuation vs. frequency over DC control voltage; measured with network analyzer (see A.6.1, parameters: $\#AVG$: 16, $IF\text{-}BW$: 10 kHz); plotted in dashed lines are the measurements from the data sheet (see [14, p. 2]) . . . 16
4.4 Measurement setup: DUT(red), RF generator/power splitter/meter(blue), DC sources/meters(green), temperature probe(yellow) . . . . . 18
4.5 Measured attenuation $A(V_{control}, f = 3\,\text{GHz})$ of the ZX73-2500-S+ as a function of the control voltage input $V_{control}$ along with the sensitivity $S(V_{control}, f = 3\,\text{GHz})$ . . . . . 20
4.6 Zoomed in version of Figure 4.5 shows the attenuation and sensitivity around the operating point $V_{control,o} = 10\,\text{V}$ . . . . . 20
4.7 Long term stability of $V_{control}$ as delivered by the Keysight 34972A DAC (ch. 205); measured with Keysight 34470A; room temperature during measurement: $\mu_\vartheta = 19.12\,°\text{C}$, $\sigma_\vartheta = 0.28\,°\text{C}$ . . . . . 21
4.8 Influence of the supply voltage $V_+$ on the attenuation . . . . . 23
4.9 Long term stability of $V_+$ as delivered by the Keysight 34972A DAC (ch. 204); measured with Keysight 34470A; room temperature during measurement: $\mu_\vartheta = 19.12\,°\text{C}$, $\sigma_\vartheta = 0.28\,°\text{C}$ . . . . . 23
4.10 Influence of an offset frequency $f - 3\,\text{GHz}$ on the attenuation . . . . . 25
4.11 Raw measurement result of the influence of the case temperature $\vartheta_{case}$ on the attenuation; color coded is the relative elapsed time of the measurement 26
4.12 Influence of the case temperature $\vartheta_{case}$ on the attenuation . . . . . 27
4.13 Comparison between the temperature stability in the "RF lab'' and inside the FLUTE LLRF cabinet . . . . . 27
4.14 Spectrum (measured with Holzworth HA7062A (subsubsection A.7.1)) showing the effect of modulating $V_{control}$ with different frequencies (Modulation amplitude: 1 V) . . . . . 29

5.1 General structure of a closed loop feedback control system . . . . . 31
5.2 Small section of the input sequence (green) and the system response (blue) 33
5.3 Step responses of the systems $\hat{G}_1(s)$, $\hat{G}_2(s)$, $\hat{G}_3(s)$ . . . . . 34
5.4 Validating the estimations $\hat{G}_1(s)$, $\hat{G}_2(s)$, $\hat{G}_3(s)$ against real data from the validation data set . . . . . 35
5.5 Block diagram of a generic PID controller . . . . . 35
5.6 Cavity power with PID controller on (before the 4.5 h mark) and off shows the stabilizing effect of the control system . . . . . 38
5.7 . . . . . 38
5.8 . . . . . 39

5.9 . . . . . 39

# List of Tables


4.1 Comparing quantization steps . . . . . 12
4.2 Requirements for the controllable RF attenuator . . . . . 15
4.3 Requirements for the controllable RF attenuator . . . . . 30

A.1 Agilent 34411A specifications . . . . . 43
A.2 Agilent 34411A some SCPI commands . . . . . 43
A.3 Keysight 34470A specifications . . . . . 43
A.4 Keysight 34470A some SCPI commands . . . . . 43
A.5 Keysight 34972A specifications . . . . . 44
A.6 Keysight 34972A some SCPI commands . . . . . 44
A.7 Tektronix MSO64 specifications . . . . . 44
A.8 Tektronix MSO64 some SCPI commands . . . . . 44
A.9 Rohde and Schwarz SMC100A specifications . . . . . 44
A.10 Rohde and Schwarz SMC100A some SCPI commands . . . . . 45
A.11 HP E4419B specifications . . . . . 45
A.12 HP E4419B some SCPI commands . . . . . 45
A.13 Agilent E5071C specifications . . . . . 45
A.14 Holzworth HA7062C specifications . . . . . 45

## Abstract

The **F**erninfrarot **L**inac- **U**nd **T**est-**E**xperiment (FLUTE), a compact linear accelerator, is currently designed and under commission at the Karlsruhe Institute of Technology (KIT). Its main purposes are to serve as a technology platform for accelerator research, the generation of strong and ultra short THz pulses and in the future as an injection device for **c**ompact **St**orage ring for **A**ccelerator **R**esearch and **T**echnology (cSTART).

At the current commissioning state, the klystron which powers the electron gun/RF cavity and in later stages the linear accelerator is fed by a pulse forming network, which is driven by a high voltage source connected to mains power. For high and a stable output power of the cavity resonator, several parameters have to be tuned to the correct values and kept inside of sometimes small tolerance bands.
In the past, the coolant temperature of the cavities water cooling system and the dependency of the pulse forming network output of the mains voltage phase were predominant sources of instability. After dealing with these issues, the cavity output power stability was improved significantly but further improvements to the stability were still desired.

In this work instead of passively optimizing the stability of system parameters, an active approach is evaluated. By controlling the amplitude of the RF input signal of klystron, which is easily possible since it is low power, the effects of noise and/or drifts are mitigated. Here it is evaluated if a simple of the shelf voltage controllable attenuator is a feasible choice to control the RF input signal, which input data should be used and which algorithm and/or control system is suitable to determine the needed attenuator setting to stabilize RF output (of the cavity).
Furthermore since the next stage in the system depends on a stable electron bunch charge rather than cavity power, it is determined whether the charge measurements of a Faraday cup can be used to directly control electron bunch charge.



## Kurzfassung

–TODO–

# 1. Introduction

# 2. Theoretical Framework

## 2.1 Linear Accelerators

In a linear particle accelerator (LINAC), charged particles such as electrons are accelerated to increase their total energy over their energy at rest.

Compared to heavier particles, such as protons ($m_p = 938.27\,\mathrm{MeV/c^2}$), electrons are fairly light ($m_p = 0.511\,\mathrm{MeV/c^2}$). Therefore they need to be brought to speeds comparable to the speed of light to achieve an useful energy increase. For this reason relativistic mechanics are needed to describe their movements[1]. [1]

With the speed of light $c = 2.998 \times 10^8\,\frac{\mathrm{m}}{\mathrm{s}}$ and the particle velocity $v$, it is common to define [2]:

$$\text{(normalized velocity)} \qquad \beta = \frac{v}{c} \tag{2.1}$$

$$\text{(relativistic mass factor)} \qquad \gamma = \frac{1}{\sqrt{1-\beta^2}} \tag{2.2}$$

The total energy of a particle is

$$U = \underbrace{(\gamma - 1)\,mc^2}_{\text{kinetic engery } W} + \underbrace{mc^2}_{\text{rest energy}} = \gamma mc^2. \tag{2.3}$$

With the kinetic electron energy out of the FLUTE electron gun of $W = 7\,\mathrm{MeV}$, rearranging Equation 2.1 and using in $W = (\gamma - 1)\,mc^2$ yield

$$\gamma = \frac{W}{m_e\,c^2} + 1 = 14.699 \tag{2.4}$$

$$\beta = \sqrt{1 - 1/\gamma^2} = 0.997\,68. \tag{2.5}$$

### 2.1.1 Some Beam Diagnostic Devices

## 2.2 Signal Analysis

### 2.2.1 Auto correlation and Cross correlation

The *cross covariance* between two stochastic processes $x[n]$ and $y[n]$ is a measure of the similarity between $x[n]$ at index $n_1$ and $y[n]$ at index $n_2$ and is defined as

$$r_{xy}[n_1, n_2] = \mathrm{E}\left\{(x[n_1] - \mu_x[n_1])(y[n_2] - \mu_y[n_2])^*\right\}. \tag{2.6}$$

[1] As relativistic mechanics are a super set of classical mechanics, the equations also apply for slower particles.

For the special case of $y[n] := x[n]$, $r_{xx}[n_1, n_2]$ is called *auto covariance* and is a measure of self similarity of $x[n]$ [3, p. 172].

The processes $x[n]$ and $y[n]$ are called *wide sense stationary* (WSS) if the following two properties hold [3, p. 167]. First, their means $\mu_\xi[n]$ are constant, i.e. they do not depend on the sample index:

$$\mu_x[n] = \mu_x \tag{2.7}$$
$$\mu_y[n] = \mu_y \tag{2.8}$$

Also the auto covariance does not depend on the absolute sample indices $n_1$ and $n_2$, but merely on the difference between them:

$$r_{xy}[n_1, n_2] = r_{xy}[m], \qquad \text{with: } m := n_2 - n_1 \tag{2.9}$$

If both process in Equation 2.6 are WSS, Equation 2.6 simplifies to

$$r_{xy}[m] = \mathrm{E}\left\{(x[n] - \mu_x)(y[n-m] - \mu_y)^*\right\}. \tag{2.10}$$

For the auto covariance both means are identical and can be moved outside the expectation operator:

$$r_{xx}[m] = \mathrm{E}\left\{(x[n])(y[n-m])^*\right\} - \mu_x^2. \tag{2.11}$$

When analyzing signals, the stochastic processes are often unknown and only one realization $x[n]$ is known. But if the process generating $x[n]$ is *(weakly) ergodic*, then one realization is enough to determine the auto covariance of the process [4, p. 252]. Then the auto covariance can be estimated with

$$\hat{r}[m] = \frac{1}{N} \sum_{n=m+1}^{N} x[n]\, x^*[n-m] \qquad m \in [0,\, N-1] \tag{2.12}$$

### 2.2.2 Estimating the Spectrum of a Stochastic Process

For a deterministic, time-discrete signal $x[n] \in \mathcal{L}_1$, the discrete Fourier transform (DFT) exists[5] and is defined as

$$X[k] = \sum_{n=0}^{N-1} x[n]\, \mathrm{e}^{-j\frac{2\pi}{N}k\,n} \qquad k, n \in [0,\, N-1], \tag{2.13}$$

using $k = \frac{N}{2\pi}\,\omega = N\,f$ as the independent, discrete frequency variable. From the complex sequence $X[k]$, often only the magnitude (or energy) is of greater interest while the phase information are neglected. Therefore, $S_{xx}$ is defined as

$$S_{xx} = |X[k]|^2 \tag{2.14}$$

and called the *energy spectral density (ESD)*.

If $x[n]$ is the realization of a stochastic process, then it is of random nature rather than deterministic. Because realizations of physical processes do not posses finite energy, they are not in the $\mathcal{L}_1$ set and their DFT is not defined [6, p. 5].

In this case instead of an energy spectral density, the spectrum of the average power of the process, called the *power spectral density (PSD)*, can be used instead. To compute the PSD, either there are two possibilities:

$$\Phi_{xx}[k] = \sum_{m=-\infty}^{\infty} r[m]\, \mathrm{e}^{-j\frac{2\pi}{N}k\,m} \tag{2.15}$$

$$\Phi_{xx}[k] = \lim_{N\to\infty} \mathrm{E}\left\{ \frac{1}{N} \left| \sum_{n=0}^{N-1} x[n]\, \mathrm{e}^{-j\frac{2\pi}{N}k\,n} \right|^2 \right\} \tag{2.16}$$

When assuming $r[m]$ decays "fast enough'', i.e.

$$\lim_{N\to\infty} \frac{1}{N} \sum_{m=-N}^{N} |m|\ |r[m]| = 0 \tag{2.17}$$

then Equation 2.15 and Equation 2.16 are equal[6, p. 7].

For measured data however neither equations can be used directly. For Equation 2.15 the auto covariance sequence $r[m]$ is unknown. But it could be estimated with Equation 2.12. In case of Equation 2.16 it is not possible to evaluate the limit, because only finite length data can be sampled and also the expectation can not be computed since in general there is only one realization available. Both operations can be neglected when doing an estimation.

With these practical changes in place, Equation 2.15 and Equation 2.16 become

$$\hat{\Phi}_{c,\,xx}[k] = \sum_{m=-(N-1)}^{N-1} \hat{r}[m]\, \mathrm{e}^{-j\frac{2\pi}{N}k\,m} \qquad \text{(Correlogram)} \tag{2.18}$$

$$\hat{\Phi}_{p,\,xx}[k] = \frac{1}{N} \left| \sum_{n=0}^{N-1} x[n]\, \mathrm{e}^{-j\frac{2\pi}{N}k\,n} \right|^2 \qquad \text{(Periodogram).} \tag{2.19}$$

Both methods yield equal results, if $r[m]$ is estimated with the biased estimator $\hat{r}[m]$ in Equation 2.12 in contrast to the unbiased estimator (compare [6, p. 24])

$$\hat{r}_{\text{unbiased}}[m] = \frac{1}{N-m} \sum_{n=m+1}^{N} x[n]\, x^*[n-m] \qquad m \in [0,\, N-1]. \tag{2.20}$$

[7] shows one key weakness of the unmodified periodogram method in Equation 2.19: The variance does not decrease significantly with more samples $N$. Instead the variance of the periodogram for each frequency approaches the square of the actual PSD:

$$\lim_{N\to\infty} \mathrm{Var}\left\{ \hat{\Phi}_{p,\,xx}[k] \right\} = \Phi_{xx}^2[k] \tag{2.21}$$

Furthermore the periodogram/correlogram suffer from the smearing and leakage effects because the limited length of the data samples always causes an implicit windowing, thus reducing frequency resolution.

There are several popular methods that improve on the periodogram/correlogram concepts:

**Blackman-Tukey:** Because of the poor accuracy of $\hat{r}[m]$ for $k \approx N$ in the definition of $\hat{\Phi}_{c,\,xx}[k]$ and the bigger the $N$, the more small errors in $\hat{r}[m]$ sum up, truncating/windowing of $\hat{r}[m]$ with $w[k]$ (length $M$) can be beneficial for the accuracy of the estimation.

$$\hat{\Phi}_{BT,\,xx}[k] = \sum_{m=-(M-1)}^{M-1} w[k]\hat{r}[m]\, \mathrm{e}^{-j\frac{2\pi}{N}k\,m} \tag{2.22}$$

The choice of the window $w[k]$ trades frequency resolution for variance and smearing for leakage reduction [6, p. 41].

**Barlett:** The Barlett method reduces the variance of the periodogram by splitting the $N$ data samples in $Q = {}^{N}/_{M}$ blocks and averaging together the sub-periodograms:

$$\hat{\Phi}_{q,\,xx}[k] = \frac{1}{M}\left|\sum_{n=0}^{M-1} x_q[n]\,\mathrm{e}^{-j\frac{2\pi}{M}k\,n}\right|^2 \tag{2.23}$$

$$\hat{\Phi}_{B,\,xx}[k] = \frac{1}{Q}\sum_{q=1}^{Q}\hat{\Phi}_{q,\,xx}[k] \tag{2.24}$$

The variance of the estimation scales with $Q$ [7, p. 6]:

$$\mathrm{Var}\left\{\hat{\Phi}_{B,\,xx}[k]\right\} = \frac{1}{Q}\Phi_{xx}^2[k] \tag{2.25}$$

**Welch:** The Welch method combines splitting the data into $Q$ segments with windowing each segment and allowing the segments to overlap. With $P = {}^{1}/_{M}\sum_{n=0}^{M-1}|w[n]|^2$ being the "power'' of the window, the Welch method is computed as

$$\hat{\Phi}_{s,\,xx}[k] = \frac{1}{MP}\left|\sum_{n=0}^{M-1} x_s[n]\,\mathrm{e}^{-j\frac{2\pi}{M}k\,n}\right|^2 \tag{2.26}$$

$$\hat{\Phi}_{W,\,xx}[k] = \frac{1}{Q}\sum_{s=1}^{Q}\hat{\Phi}_{s,\,xx}[k]. \tag{2.27}$$

Compared to the Barlett method, the overlapping of up to 50 % (see [8]) allows increasing $Q$, thus reducing the variance.

$$\mathrm{Var}\left\{\hat{\Phi}_{W,\,xx}[k]\right\} = \frac{1}{Q}\Phi_{xx}^2[k] \tag{2.28}$$

In case on a non-stationary signal $x[n]$, one possibility to analyze and display the spectral content is the use of the short time Fourier transform (STFT) and the spectrogram, which is a two dimensional power spectral density function mapping frequency and time to a third coordinate like height, intensity or color.

To calculate the spectrogram, the signal is split into segments with the sliding window $w[n-m]$ for which duration the signal is assumed to be stationary. For each segment at time index $m$, the periodogram is calculated according to

$$\hat{\Phi}_{xx}[k,m] = \frac{1}{N}\left|\sum_{n=0}^{N-1} w[n-m]x[n]\,\mathrm{e}^{-j\frac{2\pi}{N}k\,n}\right|^2. \tag{2.29}$$

## 2.3 Feedback Control Systems

# 3. Current and Needed Stability of the Electron Gun

# 4. Interfacing FLUTE

This chapter covers methods on interfacing the FLUTE accelerator, that is how to read diagnostic measurements into the control system from FLUTE and how to influence the electron acceleration appropriately to achieve stabilization.
In this chapter *input* and *output* refer to the view from the control system.

## 4.1 Inputs

FLUTE uses the *Experimental Physics and Industrial Control System (EPICS)*[9] for control of various parts of the accelerator, to send real time data to be archived and to build user interfaces via *Control System Studio (CSS)*[10], a JAVA based integrated development environment (IDE).

EPICS offers client/server and publish/subscribe paradigms to access data in so called process variables (PV) through channels. Modules are usually written in the C programming language. To ease the access to EPICS channels in programs written with the Python language, the package *PyEpics*[11] can be used. Since all data of interest as input for the control system can be extracted through an EPICS channel, the next section deals with using PyEpics to obtain the data.

### 4.1.1 Accessing EPICS channels in Python with PyEpics

Before usage PyEpics needs to be installed, e.g. with `pip3 install pyepics` from the *PyPi* repository. If the computer running the Python code can reach the EPICS CA repeater on the machine network, the connection is established automatically in the background. To get a channel value asynchronously, i.e. at an arbitrary time, the function `caget(pvname)` can be used with the name of the desired process value, see **??**.

**Listing 4.1:** Using `caget()` to get the value of an EPICS process value

```
1 from epics import caget
2 print(f"Cavity RF power: {caget('F:RF:LLRF:01:GunCav1:Power:Out')}")
```

Another way is to setup a channel object and create a subscription with an user defined callback function that is executed each time the process variable changes. This implements synchronous access to the PV and can be compared to an interrupt rather than polling the variable as in Listing 4.1.
For a non trivial example see Listing 4.2. In this program, the time differences between new values and their statistics are printed to the console.

**Listing 4.2:** Using a user defined callback function to access an EPICS process value

```
1 from epics import ca
2 import time
3 import numpy as np
```

```
4
5  dts=np.array([])
6  lastCalled=time.time()
7
8  def call(pvname, value, **kwargs):
9    global lastCalled, dts
10   now=time.time()
11   dt=now-lastCalled
12   lastCalled=now
13   dts=np.append(dts, dt)
14
15 chid=ca.create_channel("F:RF:LLRF:01:GunCav1:Power:Out")
16 _ , _ , eventID=ca.create_subscription(chid, callback=call, use_time=True)
17
18 while(True):
19   time.sleep(2)
20   print(f"N:{len(dts)},mean:{np.mean(dts)},min:{np.min(dts)},max:{np.max(dts)},std:{np.std(dts)}")
```

### 4.1.2 Properties of the Available Process Variables

In this section some process variables that may be used as inputs for the control system are analyzed. These are:

- `F:RF:LLRF:01:GunCav1:Power:Out Value`: The RF power measured immediately before the cavity
- `F:AX:DAQDT:01:1:Wave:05:Sample Value`: The charge measured with a Faraday cup (RadiaBeam Technologies FARC-04 [12]) and amplified with a charge sensitive amplifier (PCB 421A25 [13])
- `F:INJ-1:Gun:01:Temperature:Body Value`: The body temperature of the cavity

In Figure 4.1 all three are plotted for a duration of 15 min without any interference to the system and the system being in steady state operation.

In addition the sample times of the process variables is examined if the method with a custom callback is used (see Listing 4.2) or the data is extracted from the archive. The differences in the sample times are calculated according to

$$\Delta = t_{n+1} - t_n. \tag{4.1}$$

Then a histogram with the relative frequency on the y axis is used as an estimator for the probability density function of the sample time intervals (see Figure 4.2). The histogram shows that the time series resulting from recording process variables out of the EPICS system are highly unevenly spaced. Thus the data needs to be converted to posses evenly spaced sample times to use common signal processing methods like the DFT or digital LTI filters. For offline analysis of prerecorded data, it can easily be resampled to a fixed time grid. But for online operation of a filter or a whole control system it is not possible to use an arbitrary resample method because they are often non causal or introduce significant group delay when made causal. Instead calling `caget()` with a (software-) timer can be used to get evenly spaced samples online.

**Table 4.1:** Comparing quantization steps

| PV | $N_{unique}$ | $q_{avg}$ | $q_{norm}$ |
|---|---|---|---|
| F:RF:LLRF:01:GunCav1:Power:Out Value | 84 | 0.6935 | 0.011 904 |
| F:AX:DAQDT:01:1:Wave:05:Sample Value | 22 | 0.015 | 0.045 45 |
| F:INJ-1:Gun:01:Temperature:Body Value | 18 | 0.1294 | 0.055 55 |

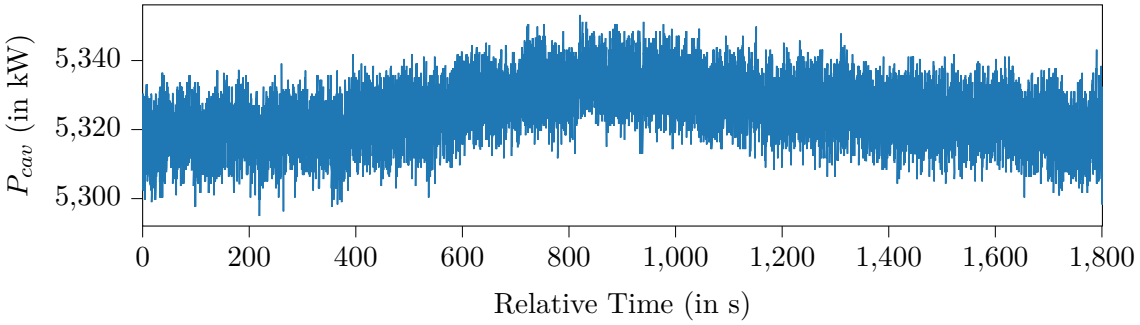


**(a)** Cavity RF power `F:RF:LLRF:01:GunCav1:Power:Out Value`

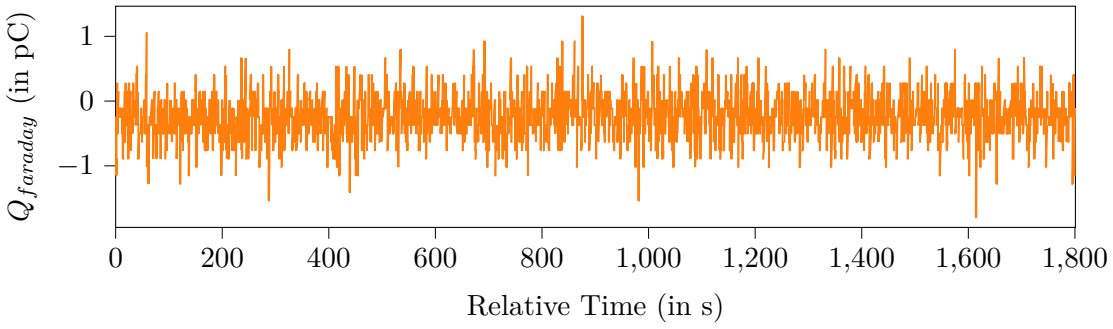


**(b)** Faraday cup charge `F:AX:DAQDT:01:1:Wave:05:Sample Value`

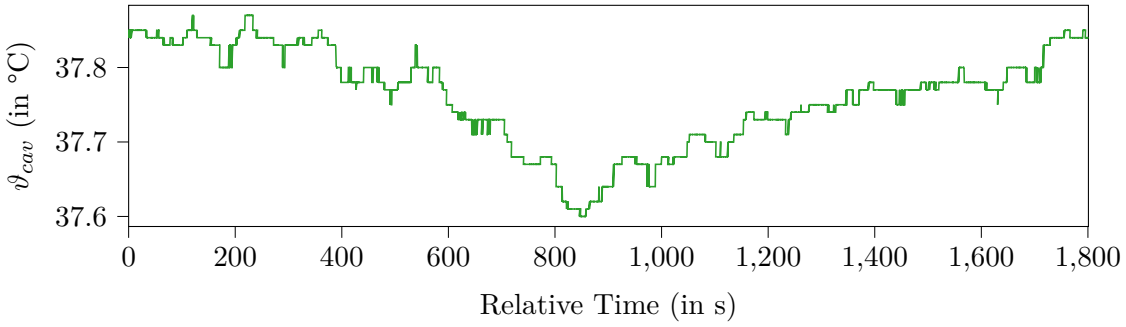


**(c)** Cavity body temperature `F:INJ-1:Gun:01:Temperature:Body Value`

**Figure 4.1:** Comparing the quantization noise of three process variables

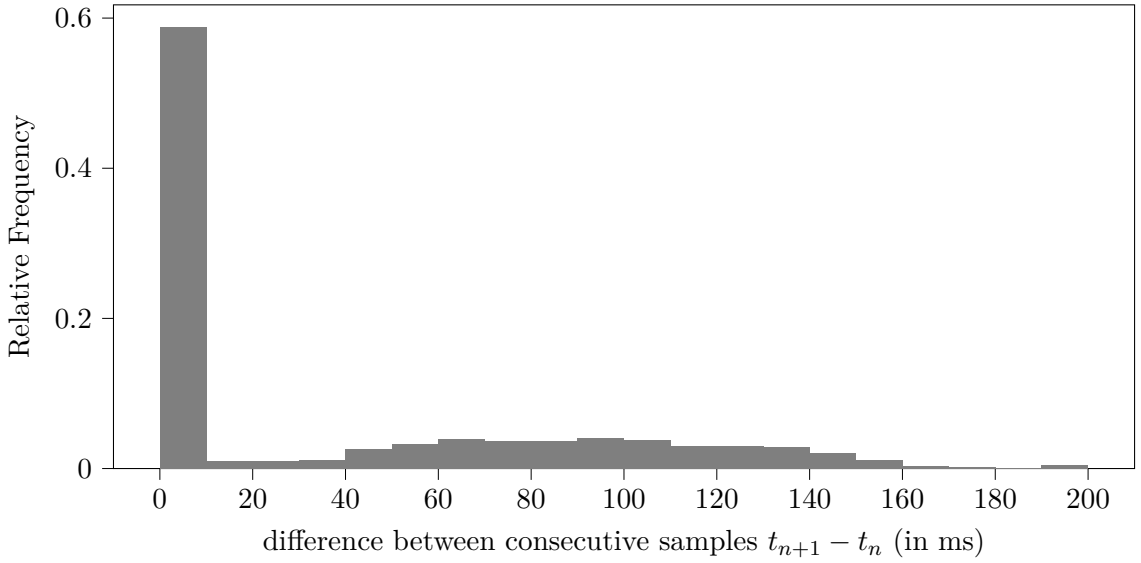


**Figure 4.2:** Histogram of the sample time intervals $\Delta$ of the plots in Figure 4.1

## 4.2 Output: Controllable RF Attenuator

The output signal computed by the control systems has to have a way of influencing the RF power send to the cavity. This could be done over an EPICS channel (e.g. with the PyEpics function `caput()` to set the value of a process variable via a channel access). However to make it possible to move the control system from a general purpose personal computer to a dedicated digital signal processor, FPGA or similar in the future, using a physical device in the signal path is preferred.

### 4.2.1 Defining Requirements

The controllable attenuator should allow to vary the attenuation in a span big enough to counteract typical instabilities on the FLUTE RF power. The set attenuation should be stable. This is especially needed in cases where the control system is not enabled. Then the attenuator should not add noise or drift to stay "transparent'' for other systems. To allow for other attenuator or amplifiers in the signal path to compensate the attenuation around its operating point, the nominal attenuation should be as low as possible. The attenuation resolution should be low enough to allow for fine control and not to add noticeable quantization noise. Also the setup time for a new value should be small enough to not be visible to the control system.

Other factors like the control/supply voltages and the operating temperature range are limited by the available hardware or governed by the mounting location.

All requirements are summarized in Table 4.2.

**Table 4.2:** Requirements for the controllable RF attenuator

| Requirement | Value/Range |
|---|---|
| attenuation adjustment | $\pm 0.2\,\mathrm{dB}$ |
| attenuation stability | $\pm 0.001\,\mathrm{dB}$ |
| nominal attenuation at operating point | $< 10\,\mathrm{dB}$ |
| attenuation resolution | $0.001\,\mathrm{dB}$ |
| setup time | $10\,\mathrm{ms}$ |
| operating temperature range | $(25.0 \pm 0.1)\,^{\circ}\mathrm{C}$ |
| supply voltage | $3\,\mathrm{V}$ to $12\,\mathrm{V}$ |
| control voltage | $3\,\mathrm{V}$ to $12\,\mathrm{V}$ |

### 4.2.2 Evaluation of the ZX73-2500-S+ Controllable RF Attenuator

The *ZX73-2500-S+* is a voltage controllable RF attenuator with coaxial SMA connectors by the company Mini-Circuits. As there is no alternative model from Mini-Circuits and devices from other manufactures are offered with similar specifications, only the ZX73-2500-S+ is evaluated in detail in this section.

The ZX73-2500-S+ attenuator consists of a brass housing/shielding containing the Mini-Circuits RVA-2500+, a variable SMD attenuator in the DV874 case form factor. The RF input and output are connected with female SMA screw connectors. The power supply and control voltage are connected with solder pins. In order to use shielded cables and a reliable connection, for all measurements SMA connectors are soldered to the supply and control pins. According to equivalent circuit in the data sheet[14] it can be assumed it is based on the common quad-$\pi$ pin diode design[15].

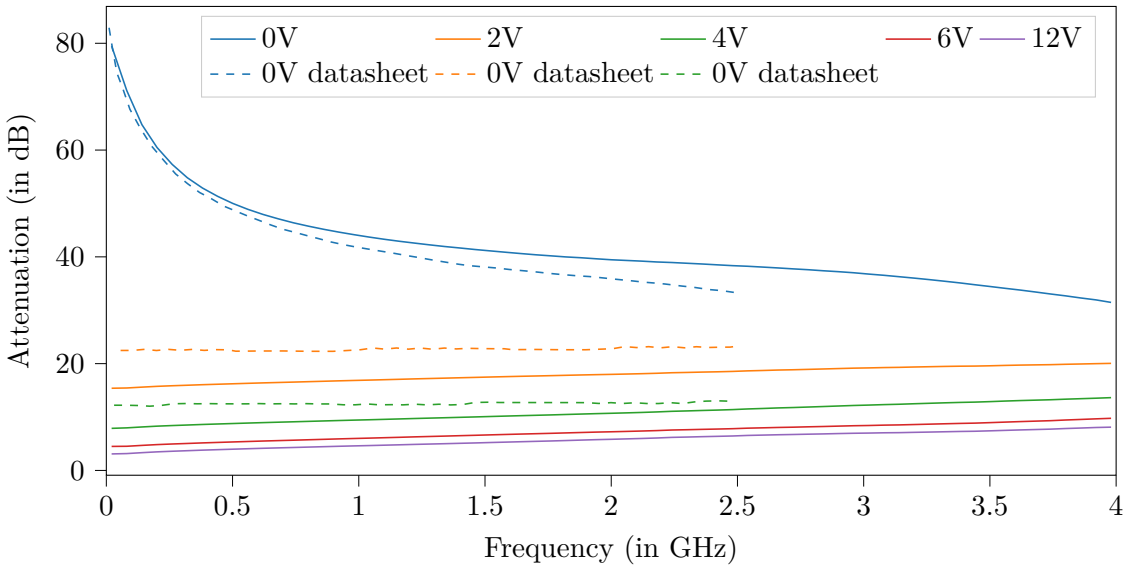


**Figure 4.3:** Attenuation vs. frequency over DC control voltage; measured with network analyzer (see A.6.1, parameters: $\#AVG$: 16, $IF\text{-}BW$: 10 kHz); plotted in dashed lines are the measurements from the data sheet (see [14, p. 2])

The attenuation versus frequency measurements from the manufactures data sheet are redone to both get a first impression of the device and verify it is generally operational and also as a sanity check for the used laboratory test equipment. Because the signal used by the FLUTE RF system is a 3 GHz single harmonic, the frequency measurement range is augmented over the maximum of 2.5 GHz in the data sheet to 4 GHz. Between the measurement of each network analyzer trace, the control voltage $V_{control}$ of the attenuator is set to 0 V, 2 V, 4 V, 6 V or 12 V. The result is shown in Figure 4.3[1]. When comparing the measured plots to the plots in the data sheet, there are obvious discrepancies. For $V_{control} = 0\,\text{V}$ the attenuator is very susceptible to noise on the control input, which could explain the differences for this curve. In the case of 2 V and 4 V, the almost constant offset scales with a similar logarithmic fashion as the attenuation does, which suggests device tolerances causing the deviations.

From this quick examination it is not possible to predict how the attenuator behaves for small changes in $V_{control}$ and how changes in the environment, such as the body temperature or the supply voltage, cause unwanted variations in the attenuation.

For this reason, with different measurement setups, the ZX73-2500-S+ is examined in greater detail in the next sections.

To compare desired and spurious influences on the attenuation, the following model is used. The attenuation of the ZX73-2500-S+ $A$ depends on the control voltage $V_{control}$ but also on the supply voltage $V+$, the case temperature $\vartheta_{case}$ and the RF frequency $f$:

$$A = A(\underbrace{V_{control},\, V_+,\, \vartheta_{case},\, f}_{\vec{x}}) = A\,(\vec{x}) \tag{4.2}$$

Other influences are not modeled as they are difficult to control, such as the manufacturing tolerances between different devices, or assumed to be negligible, such as component degradation or humidity.

[1] A through calibration of the network analyzer reduces the influence of the cables and connectors on the measurement. Change in attenuation due to play in the connectors and slight bend changes in the cables exceed the trace noise (0.004 dBrms) and cause an uncertainty of about 0.5 dB

In the next sections, the influence of each component of the parameter vector $\vec{x}$ on $A$ is measured. As a coarse approximation, all influences are assumed to have linear effect. Then the total derivative of $A$, $\Delta A$ can be written as

$$\underbrace{A(\vec{x} - \vec{x_o}) - A(\vec{x_o})}_{\Delta A} = \sum_{j=0}^{3} \frac{\Delta A}{\Delta x_j} \Delta x_j \tag{4.3}$$

where the $\Delta A/\Delta x_j$ approximate the partial derivatives $\mathrm{d}A/\mathrm{d}x_j$.

With Equation 4.3, the maximum error on the attenuation, that is the variation around the operating point with a fixed $V_{control}$, can be approximated with

$$\Delta A_{\max} = \sum_{j=0}^{3} \left| \frac{\Delta A}{\Delta x_j} \cdot \Delta x_j \right| . \tag{4.4}$$

If not specified otherwise, the operating point

$$A(\vec{x_o}) =: A_o = A(V_{control},\, V_+,\, \vartheta_{case},\, f) \tag{4.5}$$

$$A_o = A\,(10\,\mathrm{V},\, 3\,\mathrm{V},\, 20\,^\circ\mathrm{C},\, 3\,\mathrm{GHz}) \tag{4.6}$$

is used.

#### 4.2.2.1 Common Measurement Setup

For the following measurements a common setup is used to ease the recording of data and the sequential control for parameter studies. The needed tasks are:

- Supply the attenuator with the supply voltage $V_+$
- Supply the attenuator with the adjustable control voltage $V_{control}$
- Supply the RF input power with variable frequency $f$
- Measure the RF output power
- Record all data as time series to a computers storage device

To achieve this, the setup in Figure 4.4 is used. The supply and control voltage are generated by a Keysight 34972A with a 34907A module (see subsubsection A.2.1). To get a more accurate measurement of the actual voltages, two digital multimeters(Models 34470A and 34411A, see subsubsection A.1.2) are connected directly at the $V_{control}$ and $V_+$ pins. The RF signal is generated by a Rhode und Schwarz SMC 100A signal generator. With the HP E4419B and its two inputs and a power splitter, it is possible to directly get the attenuation of the ZX73-2500-S+. The body temperature of the device is monitored with a PT100 temperature sensor connected to the 34972A.

Each of the lab devices used is compatible with VXI11, which is a widely adopted standard that is used to send ASCII SCPI commands over an ethernet network (called LXI) or GPIB [16]. This enables remote and programatically control of the devices over the network. With the library *python-vxi11*, it is now possible to write a custom script, that sets the measurement devices to known initial conditions, drives the inputs of the attenuator and records the generated data. The whole setup of the hardware in **??** and the Python software, a measurement frequency of about 0.5 Hz to 1 Hz can be achieved, which is enough because most measurements taken are of a static nature and in the case of the temperature influence measurement, the thermal time constant is in the order of a few seconds. The limiting device is the HP E4419B which takes the longest to perform one measurement. Without it, measurement frequencies of over 4 Hz are possible.

All measurements are performed in the "RF lab'' in building 348 (KARA hall on KIT Campus North) which is air conditioned to about $(20 \pm 2)\,^\circ\mathrm{C}$.

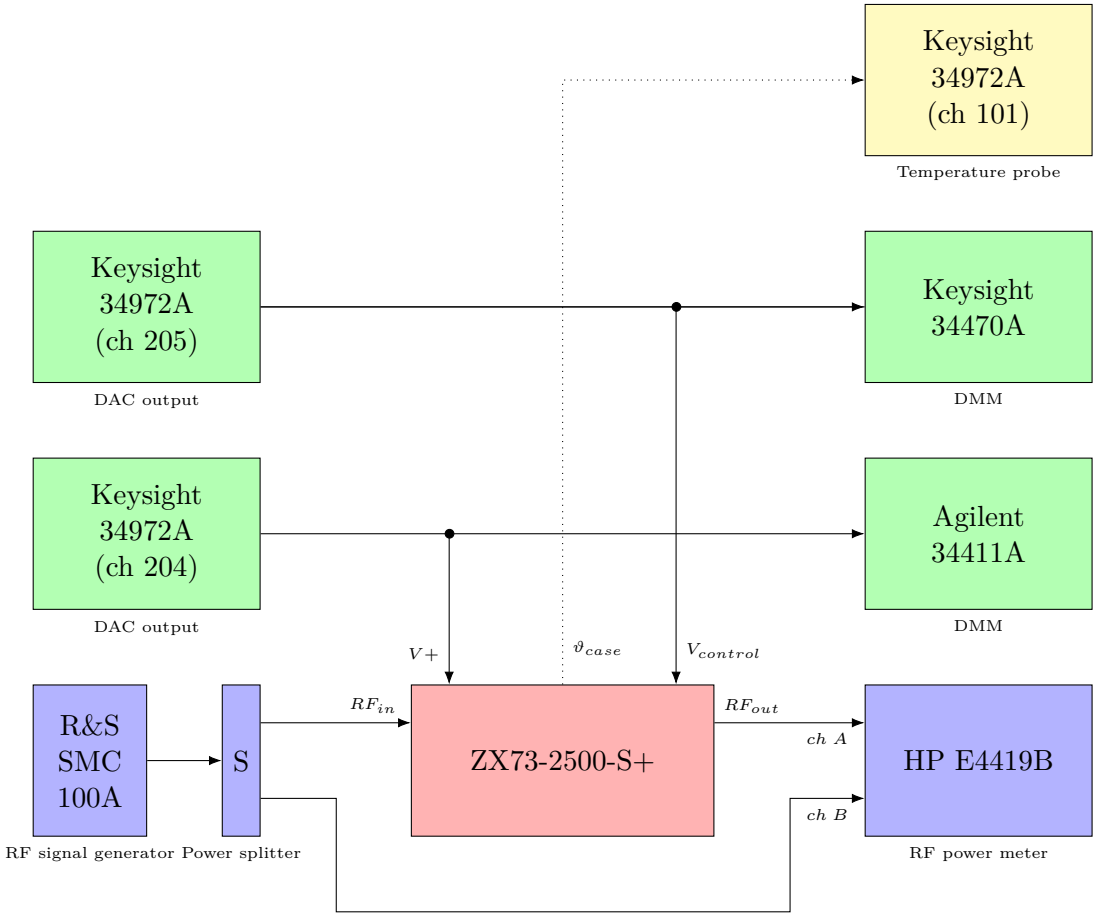


**Figure 4.4:** Measurement setup: DUT(red), RF generator/power splitter/meter(blue), DC sources/meters(green), temperature probe(yellow)

#### 4.2.2.2 Relation between Control Voltage and Attenuation

In this section the relation between the control voltage and the attenuation is examined. All other parameters are kept constant:

$$A(\vec{x}) := A(V_{control}) \tag{4.7}$$

The measured spectra in Figure 4.3 already suggest that there is a non linear relationship between the control voltage $V_{control}$ and the attenuation $A(V_{control})$ of the attenuator:

$$A(V_{control}) \neq const. \cdot V_{control} + A_0. \tag{4.8}$$

This also means the sensitivity

$$S(V_{control}) := \frac{\Delta A(V_{control})}{\Delta V_{control}} \tag{4.9}$$

is not a constant. In other words, for a desired relative change in attenuation, the needed adjustment in $V_{control}$ depends on the chosen operating point $A_o = A(V_{control,o})$.

With all other variables being at the operating point in Equation 4.5, $A(V_{control})$ is measured by stepping $V_{control}$ in 0.1 V increments up and down between 0 V and 12 V several times with each valued held constant for 30 s. $A(V_{control})$ is then calculated as the mean of all measurements $A_j(V_{control})$ with the same $V_{control}$ with

$$A(V_{control}) = \frac{1}{N} \sum_{j=0}^{N-1} A_j(V_{control}). \tag{4.10}$$

With the averaging done in Equation 4.10 and $N = 120$, the resulting mean standard deviation is $\sigma_A = 0.005\,74\,\mathrm{dB}$. Figure 4.5 shows the resulting plot.

The plot shows the attenuation can be varied over more than 30 dB and the magnitude of the sensitivity being large for small control voltages (1 V to 3 V). Since the required change in attenuation of less than 1 dB is much smaller, it is only necessary to vary $V_{control}$ around the operating point.

The optimal operating point for $V_{control}$ is selected by considering the following three aspects. First, the absolute attenuation at the operating point should be as low as possible to not worsen the SNR of the signal path. Second the control voltage has to fit in the possible output voltage range of the voltage source and still allow for adjustment towards both lower and higher voltages. In case of the Keysight 34972A/34907A the maximum possible output voltage is 12 V. Third, the sensitivity should be as low as feasible to make the attenuation less susceptible to noise on the $V_{control}$ input.

For these reasons, $V_{control,o} = 10\,\mathrm{V}$ (as already used in Equation 4.5) is chosen as the operating point, which allows $V_{control}$ to be varied in 8 V to 12 V. At the operating point $\vec{x_o}$ (with $V_{control,o} = 10\,\mathrm{V}$), the measured attenuation is

$$A(V_{control}) = 6.4859\,\mathrm{dB} \tag{4.11}$$

Figure 4.6 shows the attenuation and sensitivity around the operating point.

The sensitivity at the operating point is determined with discrete forward differentiation as

$$S(V_{control}) = S(10\,\mathrm{V}) = \frac{\Delta A}{\Delta V_{control}} = -0.151\,\frac{\mathrm{dB}}{\mathrm{V}}. \tag{4.12}$$

For further error calculations, the maximum $\Delta A(V_{control})/\Delta V_{control}$ is needed. Figure 4.6 shows the maximum magnitude of $\Delta A(V_{control})/\Delta V_{control}$ to be at the lower edge of the $V_{control}$ range of $S(8\,\mathrm{V})$:

$$\left[\frac{\Delta A(V_{control})}{\Delta V_{control}}\right]_{\max} = -0.242\,\frac{\mathrm{dB}}{\mathrm{V}} \tag{4.13}$$

The minimum possible step size of the attenuation can be calculated using $\left[\Delta A(V_{control})/\Delta V_{control}\right]_{\max}$ and the DAC output resolution of the Keysight 34907A ($^{24\,\mathrm{V}}/_{2^{16}-1} = 366.22\,\mu\mathrm{V}$):

$$\delta A(V_control) = 0.242\,\frac{\mathrm{dB}}{\mathrm{V}} \cdot 366.22\,\mu\mathrm{V} = 0.000\,088\,625\,24\,\mathrm{dB} \tag{4.14}$$

To asses the stability of $V_{control}$, delivered from the Keysight 34972A (see subsubsection A.2.1) DAC, its stability over the course of one day is measured. For that the voltage is taken once every 2 seconds with a Keysight 34470A multimeter (see subsubsection A.1.2). The result is shown in Figure 4.7.

This measurement shows the stability of $V_{control}$ to be

$$\sigma_{V_{control}} = 0.173\,\mathrm{mV} \tag{4.15}$$

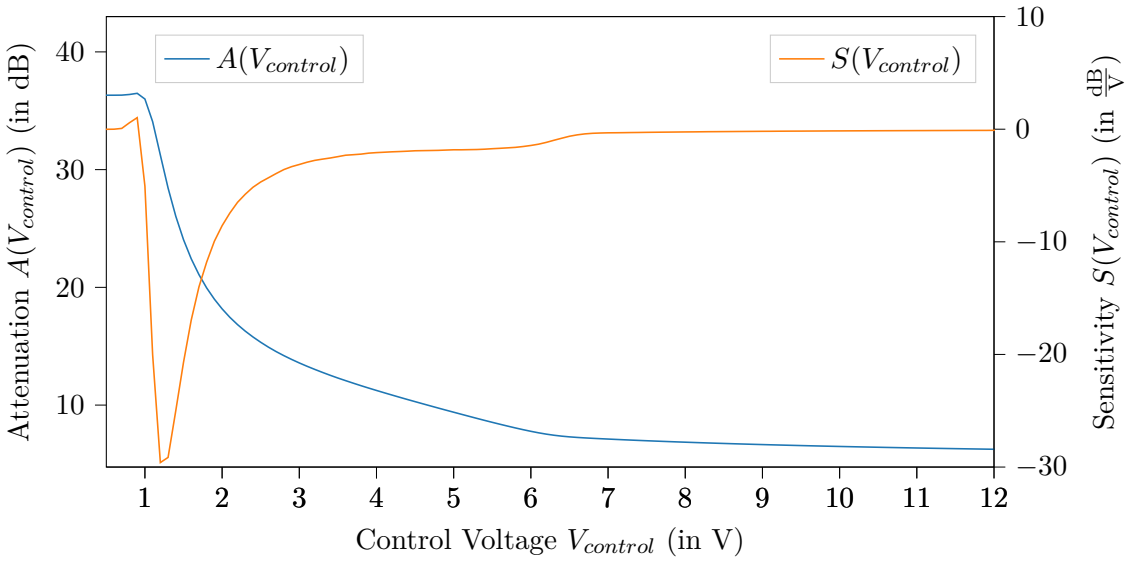


**Figure 4.5:** Measured attenuation $A(V_{control}, f = 3\,\text{GHz})$ of the ZX73-2500-S+ as a function of the control voltage input $V_{control}$ along with the sensitivity $S(V_{control}, f = 3\,\text{GHz})$

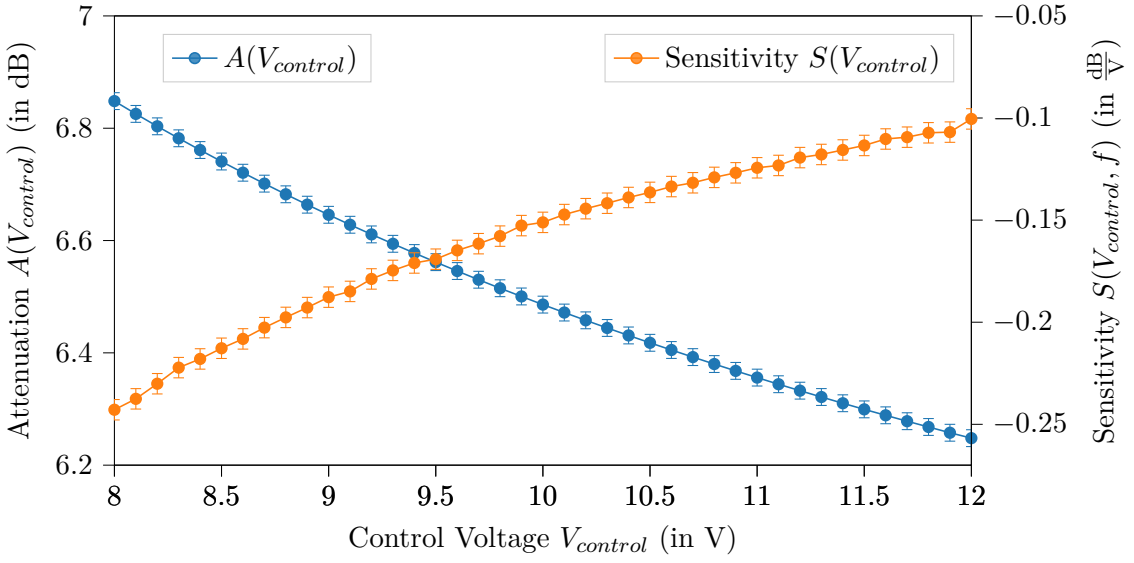


**Figure 4.6:** Zoomed in version of Figure 4.5 shows the attenuation and sensitivity around the operating point $V_{control,o} = 10\,\text{V}$

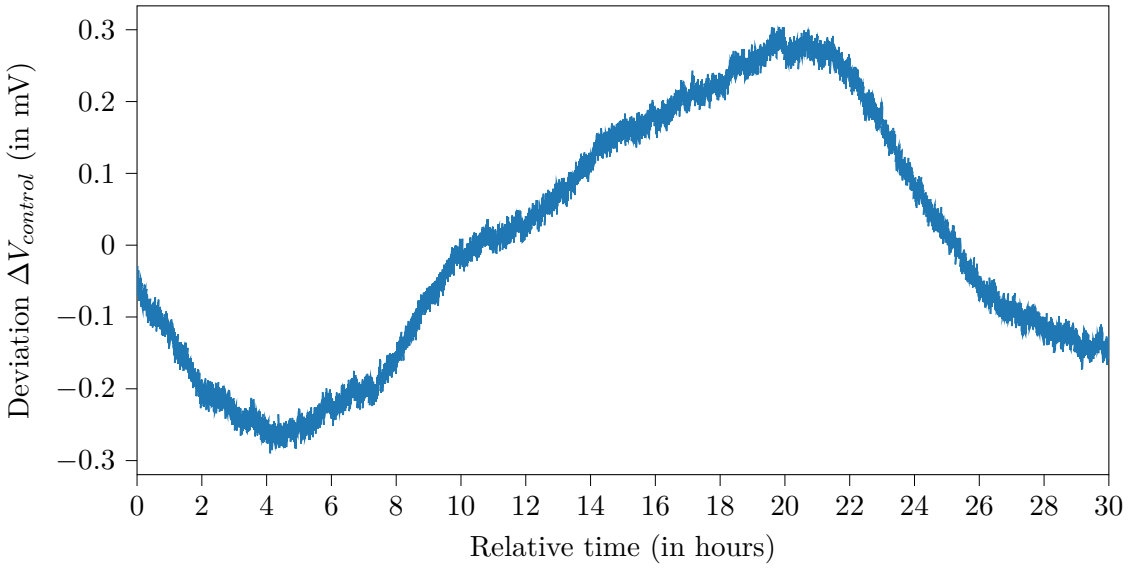


**Figure 4.7:** Long term stability of $V_{control}$ as delivered by the Keysight 34972A DAC (ch. 205); measured with Keysight 34470A;
room temperature during measurement: $\mu_\vartheta = 19.12\,°\text{C}$, $\sigma_\vartheta = 0.28\,°\text{C}$

#### 4.2.2.3 Influence of Supply Voltage Noise on Attenuation

To get the required stability for the power supply voltage, the effect of the supply voltage $V_+$ on the attenuation ${}^{\Delta A}/_{\Delta V_+}(V_+)$ has to be examined first. To do that $V+$ is varied $\pm 0.2\,\mathrm{V}$ around the nominal supply voltage at the operating point $V_{+_o} = 3\,\mathrm{V}$, all other parameters are kept constant and the attenuation is measured. To make the measurement more robust against fluctuations of the room temperature and drift of the devices, the procedure of stepping through the voltages is repeated in a similar fashion as for the influence of $V_{control}$ and the means for each set $V_+$ are computed. The result is shown in Figure 4.8.

The plot shows $A(V_+)$ to be of linear nature over the measured range. Therefore using a linear regression of the measured data points, the influence on the attenuation can be estimated to

$$\frac{\Delta A(V_+)}{\Delta V_+}(V_+) \approx \frac{\Delta A(V_+)}{V_+} = \left[\frac{\Delta A(V_+)}{V_+}\right]_{\max} = 0.003\,559\,2\,\frac{\mathrm{dB}}{\mathrm{V}}. \tag{4.16}$$

Next the stability of the supply voltage is measured. for that the stability over the course of one day is measured. The voltage is taken once every 2 seconds with a Keysight 34470A multimeter (see subsubsection A.1.2). The result is shown in Figure 4.9.

Comparing Figure 4.9 with Figure 4.7 suggest a relation between the deviations in $V_{control}$ and $V_+$. Since they are both generated by the same Keysight 34907A module, this is plausible. The slightly changing room temperature is assume to be the common cause. By calculating the correlation coefficients between $\Delta V_+$ and $\Delta V_{control}$ and also between $\Delta V_+$ and $\Delta\vartheta_{ambient}$, this can be verified:

$$\mathrm{Corr}(\Delta V_+, \Delta V_{control}) = 0.992\,04 \tag{4.17}$$

$$\mathrm{Corr}(\Delta V_+, \Delta\vartheta_{ambient}) = -0.922\,42 \tag{4.18}$$

$$\tag{4.19}$$

The long term measurement yields a standard deviation of

$$\sigma_{V,+,longterm} = 0.154\,\mathrm{mV}, \tag{4.20}$$

which is also used as the worst case stability

$$\sigma_{V_+} = 0.154\,\mathrm{mV} \tag{4.21}$$

There is also a constant offset of $\mu_{V,+,longterm} = -1.35\,\mathrm{mV}$, bu it is disregarded since it can easily be compensated for it by slightly increasing the supply voltage.

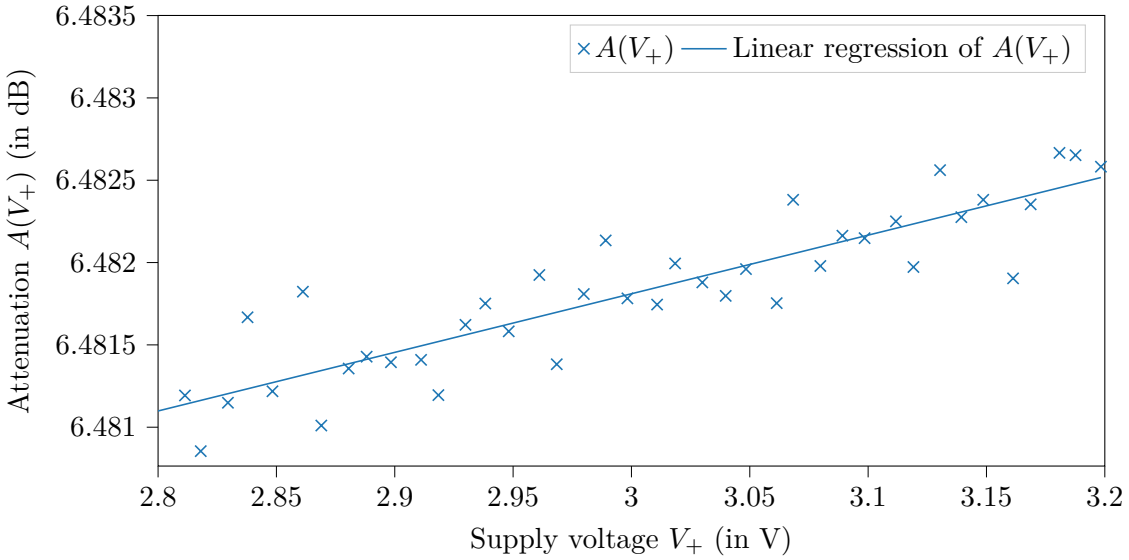


**Figure 4.8:** Influence of the supply voltage $V_+$ on the attenuation

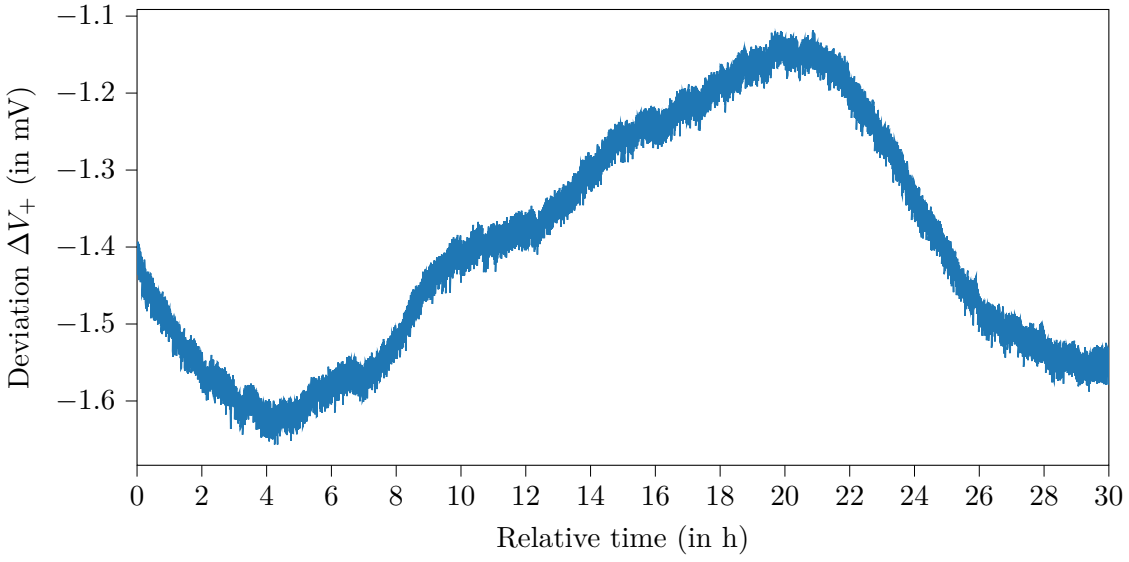


**Figure 4.9:** Long term stability of $V_+$ as delivered by the Keysight 34972A DAC (ch. 204); measured with Keysight 34470A;
room temperature during measurement: $\mu_\vartheta = 19.12\,°\mathrm{C}$, $\sigma_\vartheta = 0.28\,°\mathrm{C}$

#### 4.2.2.4 Influence of RF Frequency on Attenuation

In this section the influence of a varying RF frequency on attenuation $^{\Delta A}/_{\Delta f}(f)$ is examined. For that the set frequency of the R&S SMC100 signal generator is varied while the attenuation is measured. The result is shown in Figure 4.10.

Since the stability of the FLUTE oscillator is measured using a phase noise analyzer to be

$$\sigma_f = 0\,\mathrm{Hz}, \tag{4.22}$$

it is sufficient to regard Figure 4.10 (b). In the range of $\pm 1\,\mathrm{kHz}$ around the operating point frequency of $3\,\mathrm{GHz}$, $^{\Delta A}/_{\Delta f}(f)$ is almost constant. From the data points, the value can be calculated to

$$\frac{\Delta A(f)}{\Delta f}(f) \approx \frac{\Delta A(f)}{\Delta f} = \left[\frac{\Delta A(f)}{\Delta f}\right]_{\max} = 0.000\,004\,661\,9\,\frac{\mathrm{dB}}{\mathrm{Hz}}. \tag{4.23}$$

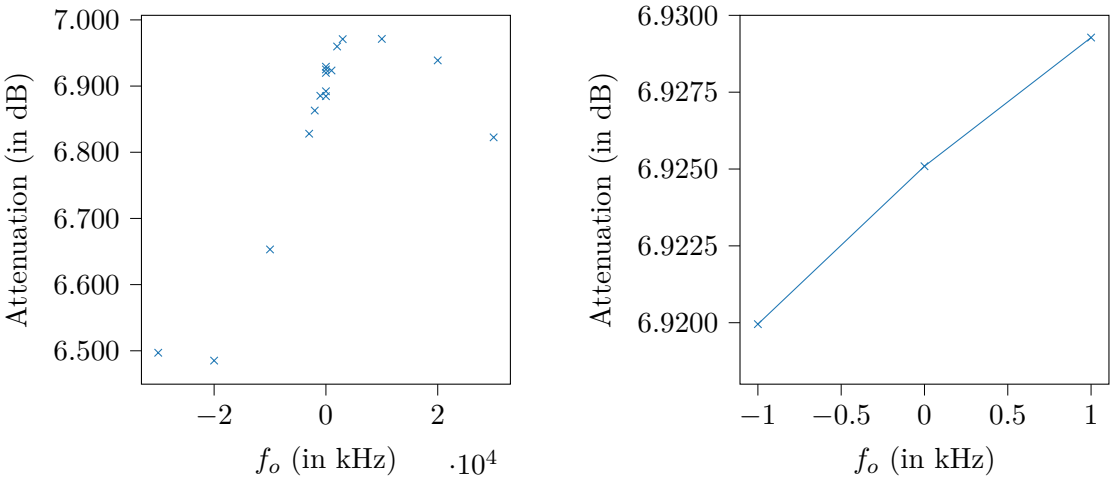


**(a)** $f = f_o \pm 30\,\text{kHz}$ **(b)** $f = f_o \pm 1\,\text{kHz}$

**Figure 4.10:** Influence of an offset frequency $f - 3\,\text{GHz}$ on the attenuation

#### 4.2.2.5 Influence of Case Temperature Variations on Attenuation

To get insight into the importance of a stable case temperature, its influence on the attenuation ${}^{\Delta A}/_{\Delta\vartheta_{case}}(\vartheta_{case})$ and the temperature stability both in the "RF lab'' and the final mounting position insight the FLUTE LLRF cabinet are measured.

To measure ${}^{\Delta A}/_{\Delta\vartheta_{case}}(\vartheta_{case})$, the following experimental setup is used.
The bottom of the attenuator is fixed to a rectangular iron profile with zip ties. Then the iron profile is heated with the tip of a soldering iron (set to 150 °C) for 1 min and then allowed to cool for 20 min. This cycle is repeated three times and the device temperature and the attenuation are measured once every 2 s. Due to heat flowing from the soldering iron to the iron profile and through device itself, a strong hysteresis between the heating and cooling cycle can be observed in Figure 4.11.

To get ${}^{\Delta A}/_{\Delta\vartheta_{case}}(\vartheta_{case})$ from the plot in Figure 4.11 an approximately linear relationship $A(\vartheta_{case})$ is assumed. To get the slope, the $\vartheta_{case}$ component of the measured data points $(\vartheta_{case}|A(\vartheta_{case}))$ are rounded to one decimal place. Then data points with the same $A(\vartheta_{case})$ are averaged together and a linear regression is applied to the result. See Figure 4.12 for the resulting plot. The linear regressor yields

$$\frac{\Delta A}{\Delta\vartheta_{case}}(\vartheta_{case}) \approx \frac{\Delta A}{\Delta\vartheta_{case}} = \left[\frac{\Delta A}{\Delta\vartheta_{case}}\right]_{\max} = 0.004\,324\,49\,\frac{\text{dB}}{\text{°C}}. \tag{4.24}$$

Next, the temperature stability in both the "RF lab'' and in the FLUTE LLRF cabinet is measured. For that in each environment the temperature is recorded over night with a thermo element connected to the Keysight 34907A inside the Keysight 34972A every two seconds.

From the data in Figure 4.13, the corresponding stabilities are calculated to be

$$\sigma_{\vartheta_{ambient,\text{RF lab}}} = 0.1067\,\text{°C} \tag{4.25}$$

$$\sigma_{\vartheta_{ambient,\text{LLRF cabinet}}} = 0.0288\,\text{°C}. \tag{4.26}$$

This assumes the case of the attenuator and the ambient around it being in thermal equilibrium. With the thick brass case and its only weakly mechanically mounting to the metal support, the attenuator posses a significant thermal time constant $\tau_{th} = R_{th}C_{th}$.

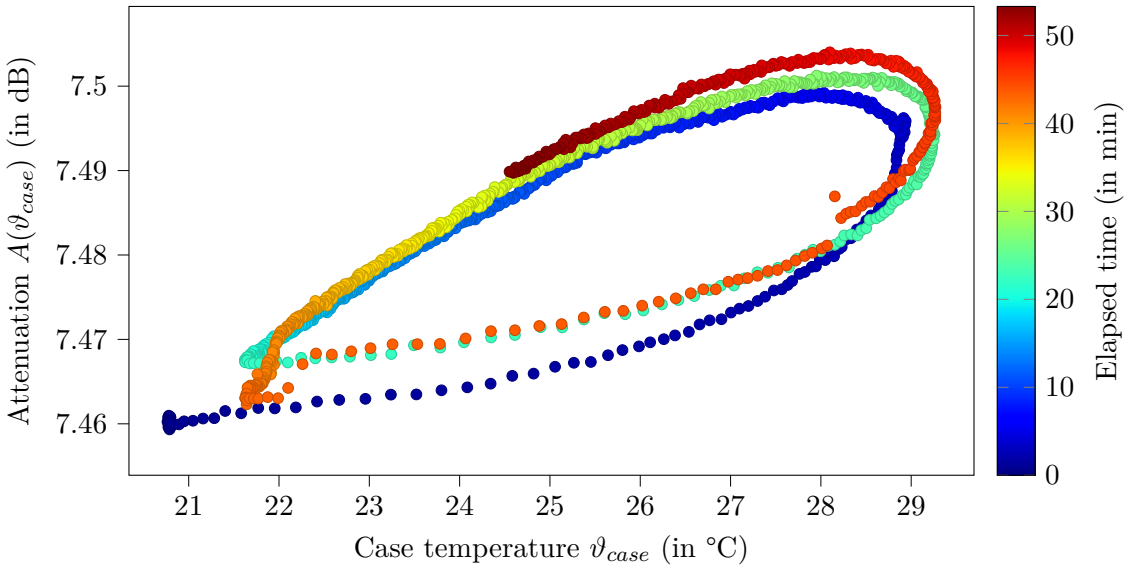


**Figure 4.11:** Raw measurement result of the influence of the case temperature $\vartheta_{case}$ on the attenuation; color coded is the relative elapsed time of the measurement

Therefore, thermally the attenuator is a lowpass filter and cannot follow fast changes in the ambient temperature. This means only slow changes of the ambient temperature have an influence on $A$, so short changes, like opening a door, have only a minor effect.

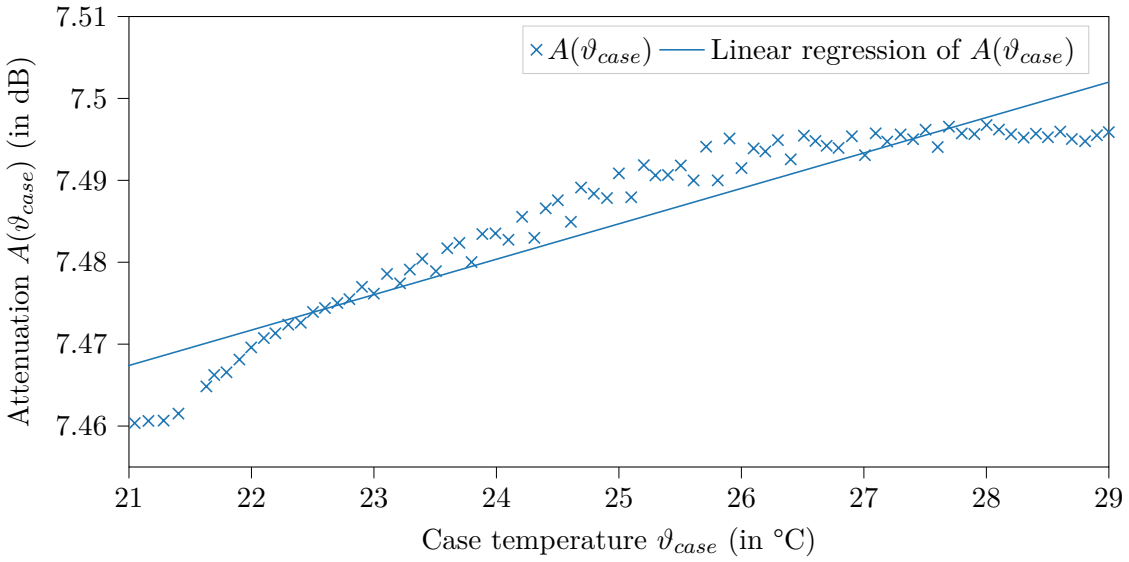


**Figure 4.12:** Influence of the case temperature $\vartheta_{case}$ on the attenuation

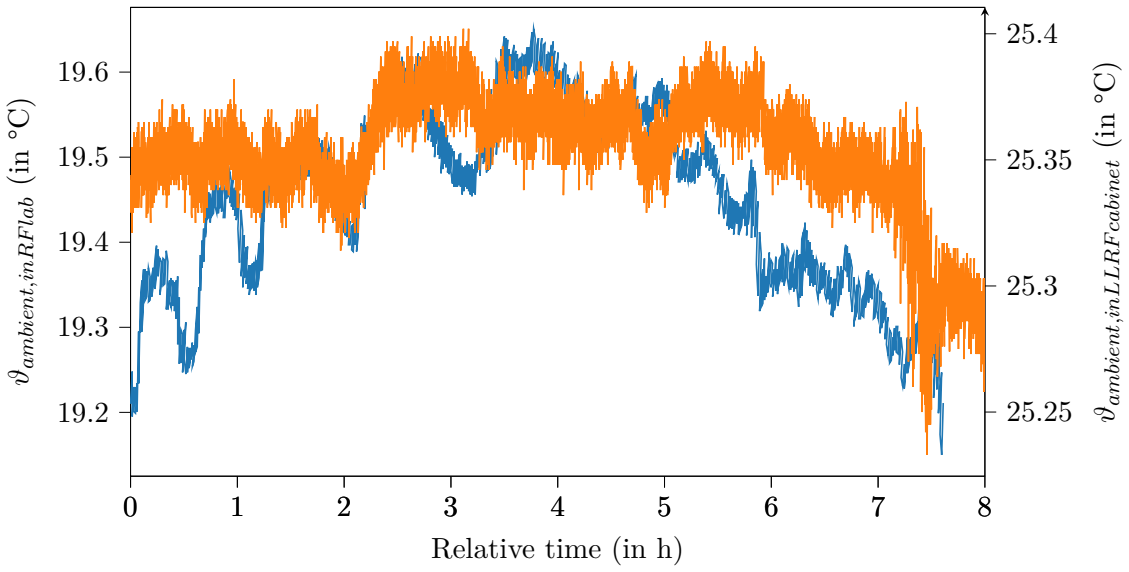


**Figure 4.13:** Comparison between the temperature stability in the "RF lab" and inside the FLUTE LLRF cabinet

#### 4.2.2.6 $V_{control}$ Frequency response

Using a non inverting adder with a *TS912IN* operational amplifier, a sine wave with constant offset is made, which is then used to drive the control voltage $V_{control}$. The result for different sine wave frequencies is shown in Figure 4.14.

This result is to be interpreted purely qualitatively, as neither measurement device and software is designed, nor is the circuit used optimal. But the traces in Figure 4.14 verify that the ZX73-2500-S+ attenuator is able to follow changes of $V_{control}$ at least up to a few ten kHz. If the attenuator should be set to a new value, this is equivalent to applying a step at the attenuators $V_{control}$ input, which according to the Fourier transform of a rect($t$) pulse, a sinc($f$) contains high frequencies.

This is at several orders of magnitude bigger than the control system can input, compute and output new values to the attenuator.

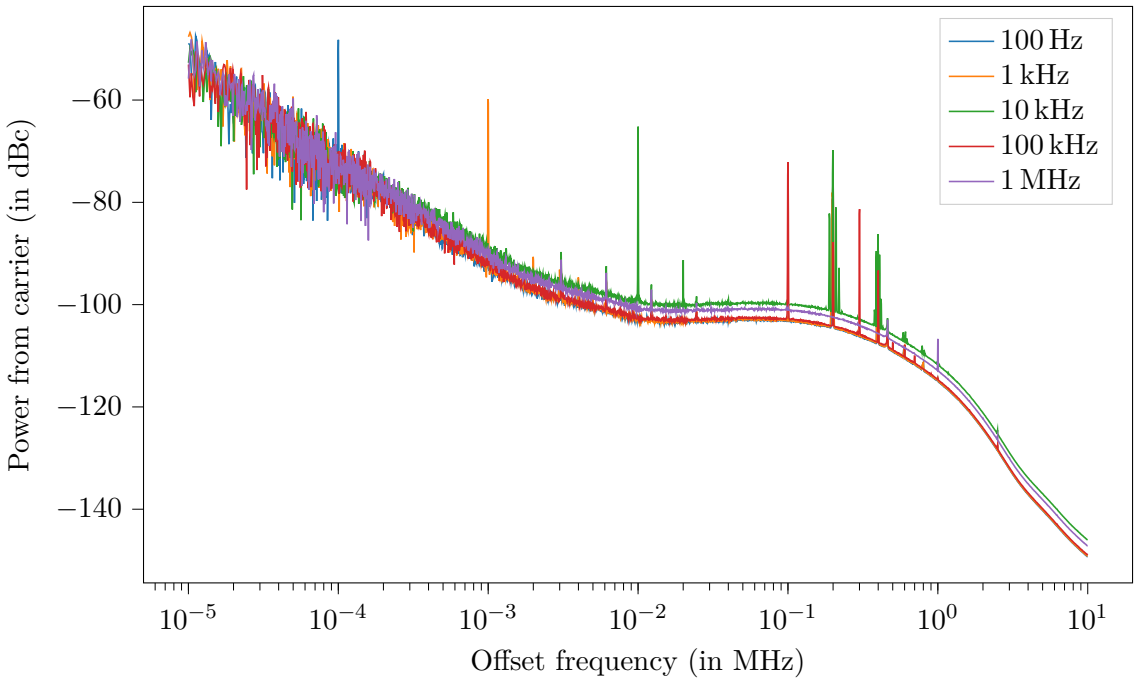


**Figure 4.14:** Spectrum (measured with Holzworth HA7062A (subsubsection A.7.1)) showing the effect of modulating $V_{control}$ with different frequencies (Modulation amplitude: 1 V)

#### 4.2.2.7 Combined Maximum Error of the Attenuation and Conclusion

Using Equation 4.4 and setting $\Delta x_j = \sigma_{x_j}$ and ${}^{\Delta A}/_{\Delta x_j} = \left[{}^{\Delta A}/_{\Delta x_j}\right]_{\max}$, the upper bound on the deviation of the attenuation, that is the error $\Delta A$ in the worst case, can now be calculated:

$$\Delta A_{\max} = \sum_{j=0}^{3} \left| \frac{\Delta A}{\Delta x_j} \cdot \Delta x_j \right| \tag{4.27}$$

$$= \left| \frac{\Delta A}{\Delta V_{control}} \cdot \Delta V_{control} \right| + \left| \frac{\Delta A}{\Delta V_{+}} \cdot \Delta V_{+} \right| + \left| \frac{\Delta A}{\Delta f} \cdot \Delta f \right| + \left| \frac{\Delta A}{\Delta \vartheta_{case}} \cdot \Delta \vartheta_{case} \right| \tag{4.28}$$

$$= \underbrace{0.242\,\frac{\mathrm{dB}}{\mathrm{V}} \cdot 0.173\,\mathrm{mV}}_{41.9\,\mu\mathrm{dB}} \tag{4.29}$$

$$+ \underbrace{0.003\,559\,2\,\frac{\mathrm{dB}}{\mathrm{V}} \cdot 0.154\,\mathrm{mV}}_{548\,\mathrm{ndB}} \tag{4.30}$$

$$+ \underbrace{0.000\,004\,66\,\frac{\mathrm{dB}}{\mathrm{Hz}} \cdot 0\,\mathrm{Hz}}_{0\,\mathrm{dB}} \tag{4.31}$$

$$+ \underbrace{0.004\,325\,\frac{\mathrm{dB}}{^{\circ}\mathrm{C}} \cdot 0.11\,^{\circ}\mathrm{C}}_{475.75\,\mu\mathrm{dB}} \tag{4.32}$$

$$= 518\,\mu\mathrm{dB} = 0.000\,518\,\mathrm{dB} \tag{4.33}$$

This shows even in the worst case, the ZX73-2500-S+ attenuator is stable within the requirement.

The other requirements from Table 4.2 are also fulfilled, see Table 4.3.

**Table 4.3:** Requirements for the controllable RF attenuator

| Requirement | Value/Range set | Value/Range actual | Verdict |
|---|---|---|---|
| attenuation adjustment | $\geq \pm 0.2\,\mathrm{dB}$ | $\pm 0.3\,\mathrm{dB}$ | pass |
| attenuation stability | $\leq \pm 0.001\,\mathrm{dB}$ | $0.000\,518\,\mathrm{dB}$ | pass |
| nominal attenuation at operating point | $\leq 10\,\mathrm{dB}$ | $6.6\,\mathrm{dB}$ | pass |
| attenuation resolution | $\leq 0.001\,\mathrm{dB}$ | $0.000\,089\,\mathrm{dB}$ | pass |
| setup time | $\leq 10\,\mathrm{ms}$ | $1\,\mathrm{ms}$ | pass |
| operating temperature range | $(25.0 \pm 0.1)\,^{\circ}\mathrm{C}$ | $(25.0 \pm 0.1)\,^{\circ}\mathrm{C}$ | pass |
| supply voltage | $3\,\mathrm{V}$ to $12\,\mathrm{V}$ | $3\,\mathrm{V}$ | pass |
| control voltage | $3\,\mathrm{V}$ to $12\,\mathrm{V}$ | $8\,\mathrm{V}$ to $12\,\mathrm{V}$ | pass |

# 5. Controller Design and Evaluation

In this chapter stabilizing the power output of FLUTE by means of a control system is examined. This is different than previous attempts in that a feedback control system tries to compensate short term disturbances and long term drifts *actively* by interfering with some part of FLUTE that has influence of the output power.

The next sections describe the chosen architecture of a suitable control system as well as some implementation details and the tuning of necessary controller parameters.

## 5.1 Architecture

The general structure of a closed loop control system is shown in Figure 5.1.

$y(t)$ is the physical quantity which should follow a certain time trajectory $x(t)$ or be kept constant (then $x(t) = x = const.$). If there are no disturbances $d(t)$ or the disturbances are deterministic (i.e. $d(t)$ is known $\forall t$), then an open loop system would be possible. In that case the role of the controller would be to merely to set its output $u(t)$ according to the system dynamics of the plant[1] (represented by its impulse response $g(t)$).

In most real world scenarios, $d(t)$ originates from a stochastic process and thus is unknown. Too remedy the negative influences of $d(t)$, the output $y(t)$ is measured and feed back. Based on the error $e(t)$, which is the difference between the set value and the actual value defined by

$$e(t) = x(t) - y(t), \tag{5.1}$$

the controller can react accordingly.

[1] Assuming $g(t)$ is a stable LTI system

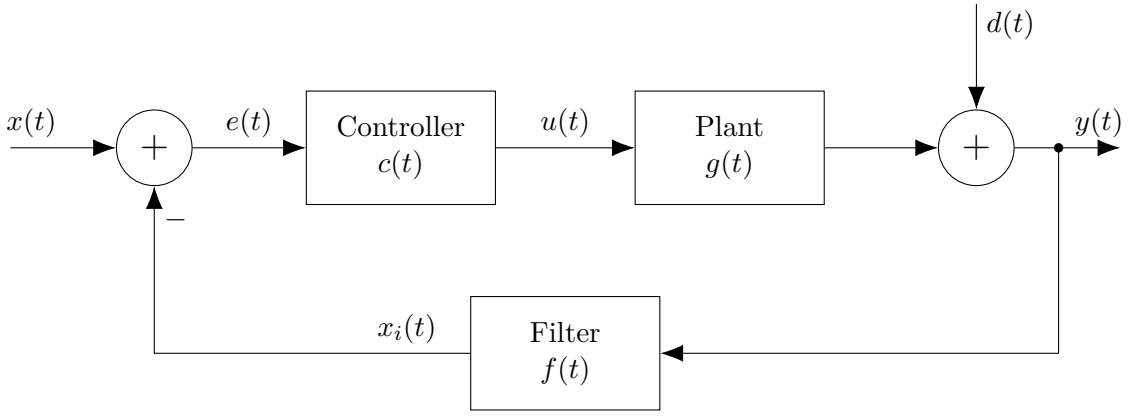


**Figure 5.1:** General structure of a closed loop feedback control system

## 5.2 Inputs and Outputs

Since the control algorithm should be implemented, tested and used online on the actual accelerator instead of only operate on simulated data, there is the need for fast and reliable interfaces to the machine. Following, "input'' refers to the signal going into the control algorithm (i.e. the measured $y(t)$), while "output'' is the output of the control algorithm $u(t)$.

### 5.2.1 Input

Depending on which value is chosen to be controlled, filtering of the input signal could be mandatory.

In the case of the cavity RF power the signal jumps to zero each time a breakdown occurs, shortening the RF supply. These outliners are not representative of the average RF power inside the cavity over multiple pulses and thus would greatly impair the controller performance. For that reason, before any further filtering to remove noise etc, a breakdown removal filter is used (Listing 5.1). In principle the new power value is checked to be inside a band which size is determined by the mean deviation of the $N_{filt}$ previous values and a scaling $m$. The percentile differences are used here as they are robust against outliners (i.e. other breakdowns) in the $N_{filt}$ previous values opposed to a normal standard deviation. The scaling with $(2 * 1.2815)^{-1}$ is used to make the mean deviation comparable to a standard deviation.

**Listing 5.1:** Breakdown removal

```
{}↓...
if(abs(P[i]−np.median(P[i−3∗Nfilt:i−Nfilt]))<
m∗(np.percentile(P[i−3∗Nfilt:i−Nfilt],90)−np.percentile(P[i−3∗Nfilt:i−Nfilt],10)/(2∗1.2815))):
    P_filt =np.append(P_filt,P[i])
else:
    breakdown_locations_predicted=np.append(breakdown_locations_predicted,i)
    P_filt =np.append(P_filt,np.median(P[i−3∗Nfilt:i−Nfilt]))
#...
```

### 5.2.2 Output

For the control system to work the controller needs some way of influencing the plant. For that the output of the FLUTE LLRF vector modulator is controlled by a RF attenuator (see **??**).

## 5.3 Plant Identification

### 5.3.1 Principle

Before choosing an appropriate controller, some insight of the system response has to be obtained. For that reason, next the plant transfer function is obtained. In the time domain, the transfer function is the response of the system to an impulse on the input. So per definition, in the special case here, this would mean changing the RF attenuator quickly from a big attenuation to a small attenuation and then back. This is not easy to measure and a single measurement is very susceptible to noise. Therefore it is more common to measure the step response instead and to average over several step responses.

When there is no prior knowledge over the system, the identification is sometimes done with a (pseudo) random binary sequence to excite the system with step functions of different lengths. Then it is necessary that some of the steps last longer than a few dominant time constants of the system. To get the transfer function of the system from its step response, several methods are common, including correlation based and frequency response based algorithms.

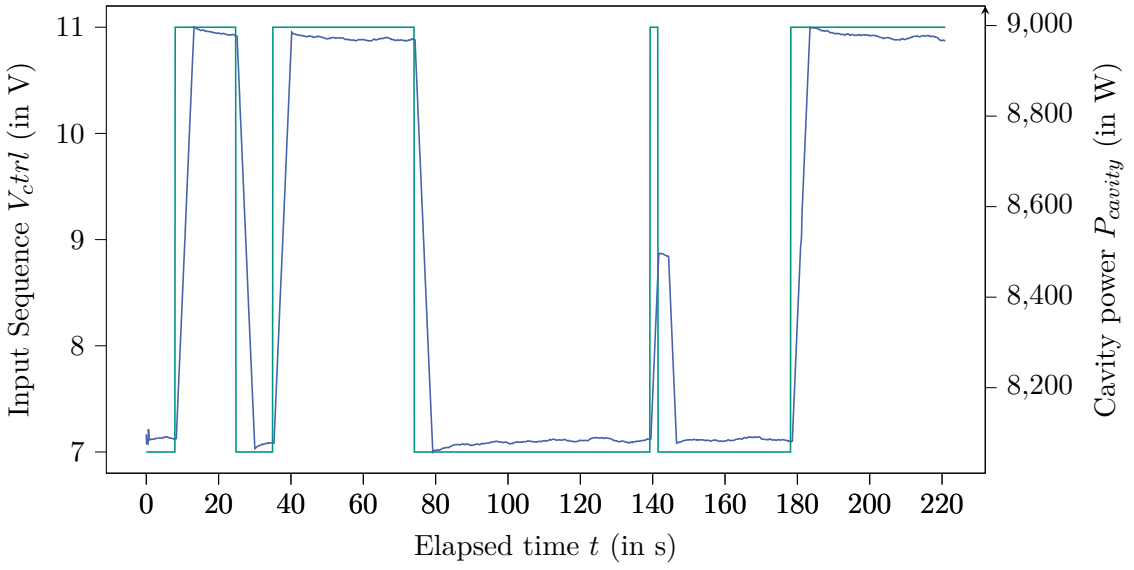


**Figure 5.2:** Small section of the input sequence (green) and the system response (blue)

### 5.3.2 Identifying the system response of the FLUTE LLRF

The input sequence is generated by modulating the RF attenuator around a base attenuation. As a trade off between high SNR and driving the LLRF in a "save" region, the control voltage span is chosen to be 4 V in total (7 V to 11 V around the base control voltage of 9 V).

To get a random binary sequence, depending on the outcome of a binomial random process, the voltage is toggled between 7 V and 11 V according to Listing 5.2. With the parameter `toggleP`, the average length of one constant voltage level can be controlled.

**Listing 5.2:** Function to get a random binary sequence

```
1 def randomBinarySequence(N,toggleP):
2     u=[False]*N
3     for i in range(1,len(u)):
4         if(np.random.binomial(1,toggleP,1)[0]):
5             u[i]=not u[i-1]
6         else:
7             u[i]=u[i-1]
8     return list(map(lambda x: 7 if x==False else 11,u))
```

In a test run over 6 hours (after FLUTE had stabilized), the attenuator was driven with such a random sequence. The result is shown in Figure 5.2.

The time signals are then split into a estimation data set (about 80 % of samples) and a validation data set (the remaining ≈ 20 %).

The two data sets are then loaded into the {}<MATLAB *System Identification Toolbox* (SIT). With the SIT, first the means of both sets and both the input and output are removed, which is required by the estimators used. Then with different numbers of poles and zeros, the transfer function is estimated. After trying several settings, three promising candidates

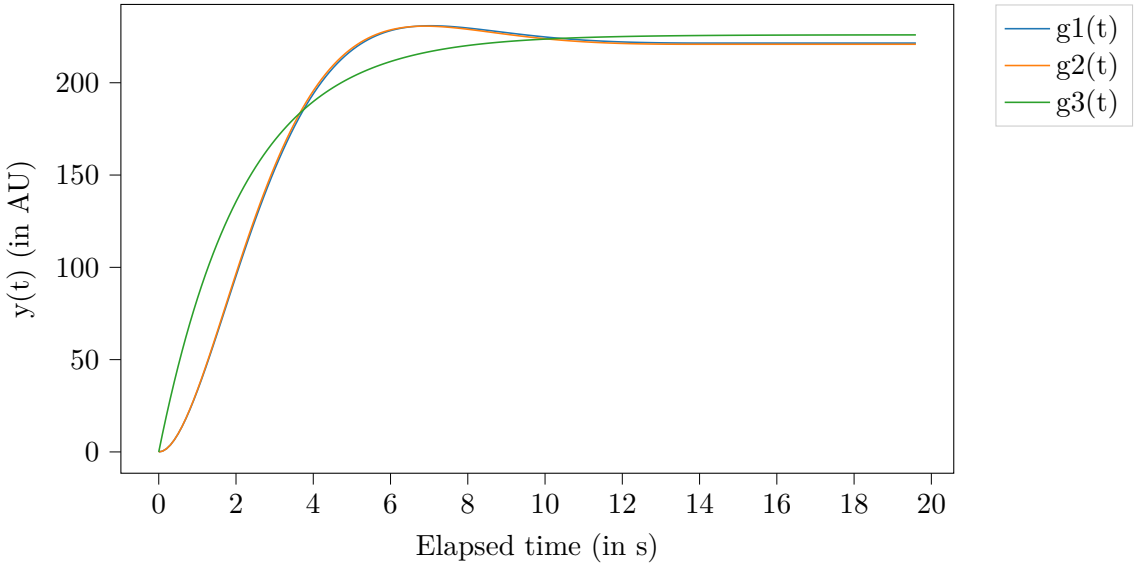


**Figure 5.3:** Step responses of the systems $\hat{G}_1(s)$, $\hat{G}_2(s)$, $\hat{G}_3(s)$

$$\hat{G}_1(s) = \frac{71.37\,s + 0.5966}{s^3 + 0.8208\,s^2 + 0.328\,s + 0.002733} \tag{5.2}$$

$$\hat{G}_2(s) = \frac{-0.2125\,s + 70.85}{s^2 + 0.8022\,s + 0.3202} \tag{5.3}$$

$$\hat{G}_3(s) = \frac{79.12}{s + 0.3502} \tag{5.4}$$

emerge.

For these transfer functions, the (single) step responses are given in Figure 5.3.

To check the accuracy of the estimations, the SIT is used to do a simulation with the $\hat{G}_i(s)$ and the validation data set (see Figure 5.4).

Figure 5.4 shows that a first order system with one pole and no zeros is not a sufficient approximation as there is no overshoot, since it is not possible in a first order system. The second and third order systems $\hat{G}_2(s)$ and $\hat{G}_3(s)$ show much better fits.

The important conclusion of this section is that the plant can be modeled as a **second order system**. This info is needed when choosing a controller in the next section.

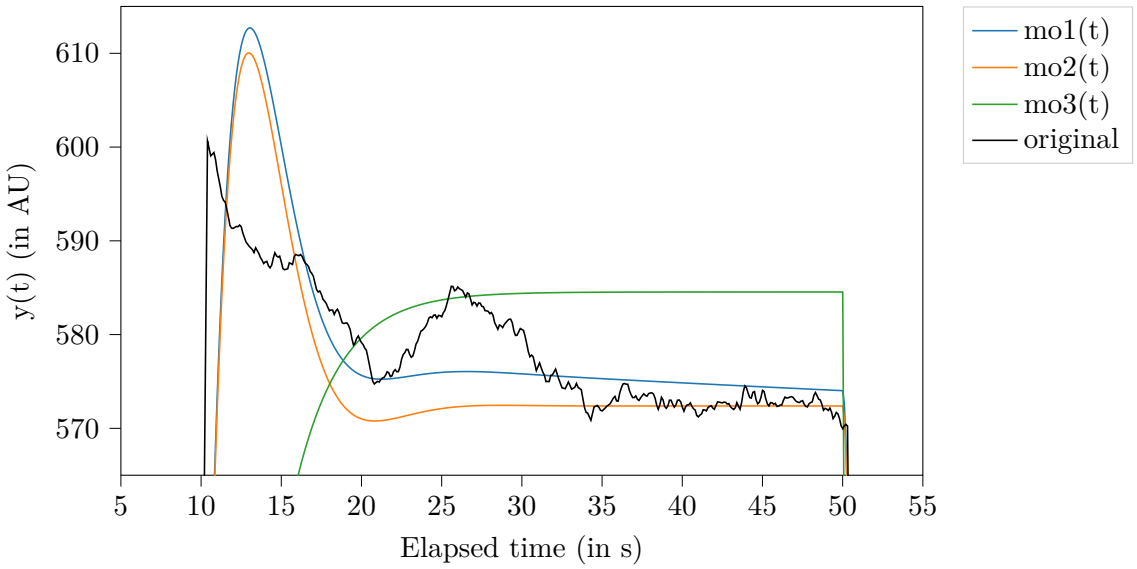


**Figure 5.4:** Validating the estimations $\hat{G}_1(s)$, $\hat{G}_2(s)$, $\hat{G}_3(s)$ against real data from the validation data set

## 5.4 Controller design

For many control problems, especially if the plant behaves approximately as an LTI system and the system is of low order, a simple PID (proportional, integral and derivative) controller is a good starting point (visualized in Figure 5.5).

A PID controller uses the error $e(t)$, the temporal integral of the error $e_i(t)$ and the temporal derivative of the error $e_d(t)$ as an input and outputs a weighed sum of them. While the unmodified error signal represents the current error, the integrated and derived error signals allow to controller to "see" in the past and predict the future.

Often simplifications, such as a pure P (only $k_p \neq 0$) or a PI (only $k_p$, $k_i \neq 0$) controller are valid as well. Since the plant has been identified to be a second order system, a simple P controller is not enough to bring the steady state error to zero (see ). So at least a PI controller is needed.

As a starting point for software development and parameter tuning, the parameters $k_p = 0.00001$ and $k_i = k_d = 0$ are chosen. This ensures during development the system basically does nothing but still shows changing values at the controller output.

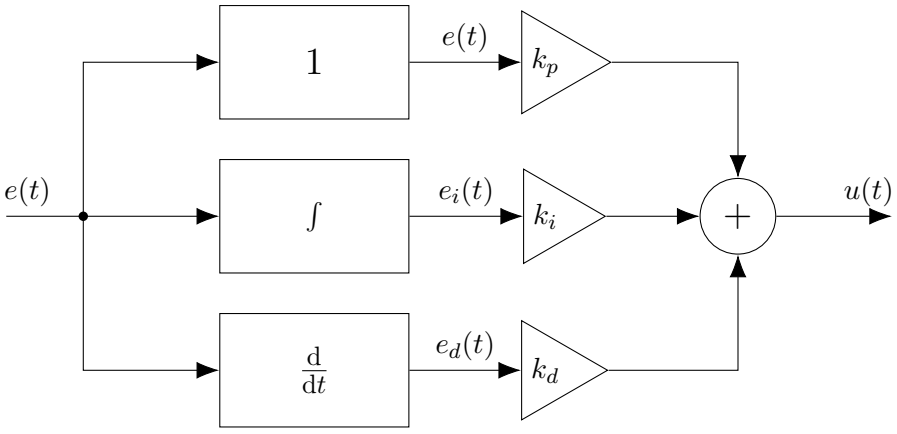


**Figure 5.5:** Block diagram of a generic PID controller

## 5.5 Software Design

As integrating a new subsystem into EPICS takes some time and effort and the control system is designated a temporary solution, it is more viable to operate it as an independent system.

Before choosing a programming language, software frameworks, etc. the key requirements for the software are discussed:

- Communication with EPICS to get values and with the RF attenuator
- Efficient and lightweight to achieve clock cycles times of a most 0.1 s
- Easy implementation of a (time discrete) PID controller
- GUI to show input, output and error signals
- Possibility to log signals to file for documentation

With these in mind first programming languages are regarded. As there are EPICS libraries for both C++ and Python, these two languages are examined in more detail.
While C++ as a compile language promises speed, all other requirements are possible but would take much greater effort in C++ compared to Python. For that reason, in the following a small test program is written to evaluate the fastest clock cycle possible with a simple Python program.

shows that retrieving one value of an EPICS channel and setting a new attenuator voltage takes only about 20 ms, thus using C++ is not necessary and Python can be utilized instead.

To create a PID controller in software instead of a continuous time system, only discrete time implementations are possible. Choosing a high clock cycle frequency however approximates the continuous time system. To get the error signals for the integral and derivative part, the integral is replaced with a cumulative recursive sum as

$$e_i[n] = e_i[n-1] + e[n] \cdot dt, \tag{5.5}$$

while the derivative is replaced by a difference

$$e_d[n] = \frac{e_i[n-1] - e[n]}{dt}. \tag{5.6}$$

For the GUI a common framework should be used. In Python Tk and wxwidgets are common ways to build a GUI. Another viable option is PyQt, which, as the name suggests, is a Python port of the Qt framework. One major advantage of using PyQt is the possibility to import `.ui` files describing the GUI directly from the Qt RAD designer called "Qt designer'', removing the need to create the GUI programmatically. Furthermore using PyQt enables the usage of *pyqtgraph*, a highspeed plotting library only compatible with Qt. This ensures plotting live data does not bottleneck performance, which is often the problem with naive *matplotlib* based solutions.

To log all relevant data from RAM to non-volatile memory (hard drive or network share), a simple approach with a line by line CSV writer is used.

## 5.6 Control Parameter Tuning and Tests

To tune control parameters there are a multiple of analytical, empirical or hybrid approaches. Here the Ziegler-Nichols method is tested and fine tuning is done by hand.

## 5.7 Results

As Figure 5.6 shows, with the control system activated, the standard deviation drops from about 150 W to less than 10 W, which shows the effectiveness of the system.

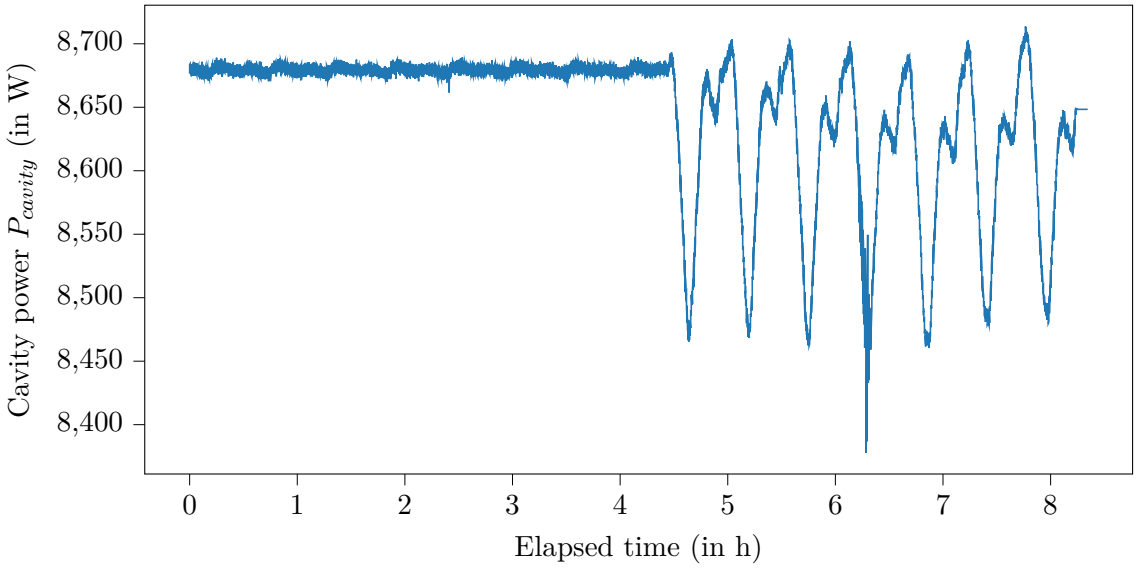


**Figure 5.6:** Cavity power with PID controller on (before the 4.5 h mark) and off shows the stabilizing effect of the control system

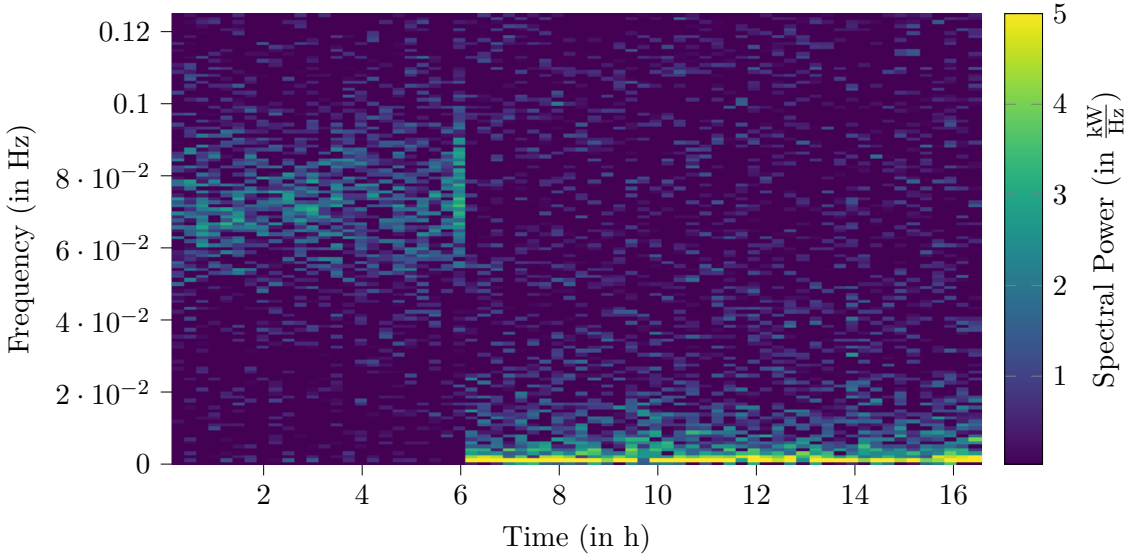


**Figure 5.7**

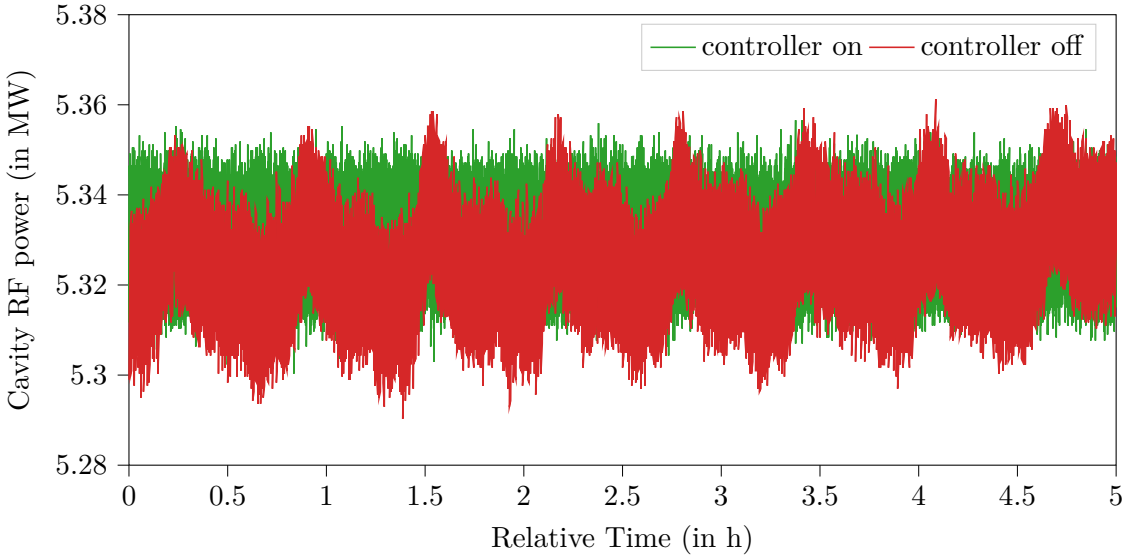


**Figure 5.8**

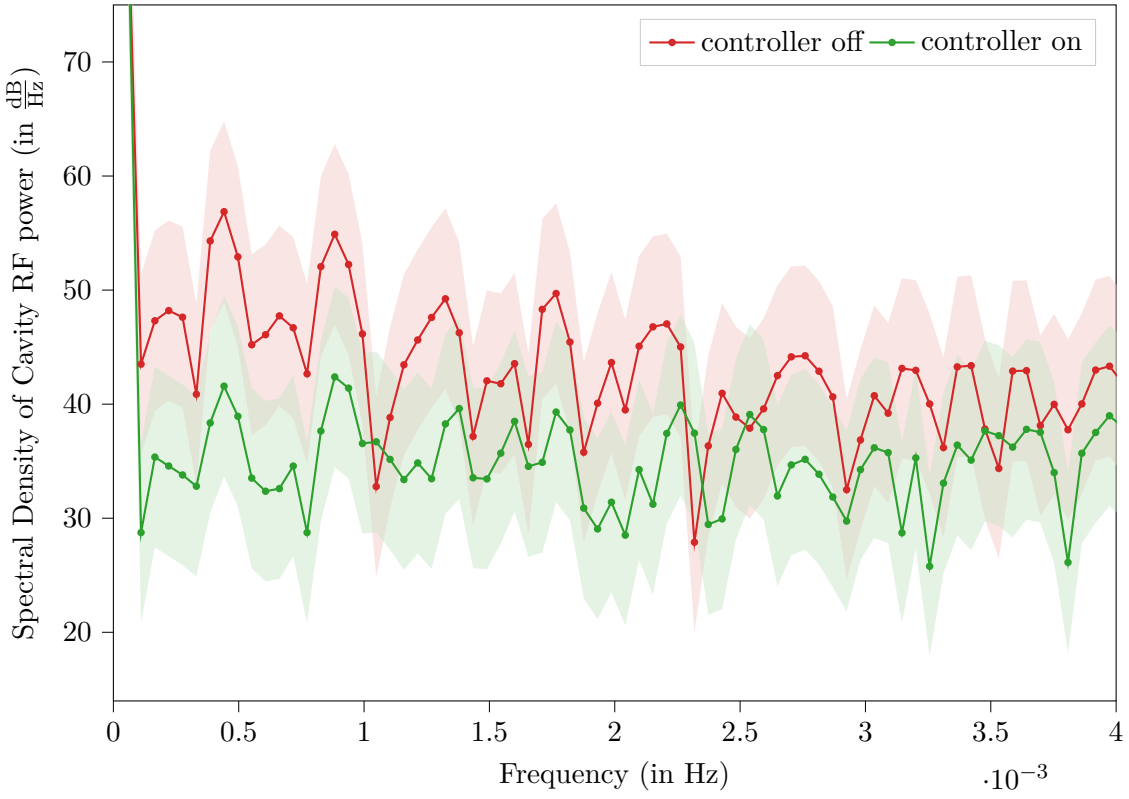


**Figure 5.9**

# 6. Summary and Outlook

# Appendix

## A Lab Test and Measurement Equipment

### A.1 Benchtop multimeters

#### A.1.1 Agilent 34411A

**Table A.1:** Agilent 34411A specifications

| **Specification** | **Value** |
|---|---|
| | DC volt |
| Digits | 6 1/2 |
| Measurement method | cont integrating multi-slope IV A/D converter |
| Accuracy (10 V range, 24 hours) | 0.0015 %+0.0004 % (% of reading + % of range) |
| Bandwidth | 15 kHz (typ.) |

**Table A.2:** Agilent 34411A some SCPI commands

| **Description** | **Example command** | **Example return** |
|---|---|---|
| Read current measurement | `READ?` | `+2.84829881E+00` (2.848 V) |

#### A.1.2 Keysight 34470A

**Table A.3:** Keysight 34470A specifications

| **Specification** | **Value** |
|---|---|
| | DC volt |
| Digits | 7 1/2 |
| Measurement method | cont integrating multi-slope IV A/D converter |
| Accuracy (10 V range, 24 hours) | 0.0008 %+0.0002 % (% of reading + % of range) |
| Bandwidth (10 V range) | 15 kHz (typ.) |

**Table A.4:** Keysight 34470A some SCPI commands

| **Description** | **Example command** | **Example return** |
|---|---|---|
| Read current measurement | `READ?` | `+9.99710196E+00` (9.997 V) |

## A.2 Data Acquisition/Switch Unit

### A.2.1 Keysight 34972A

**Table A.5:** Keysight 34972A specifications

| Specification | Value |
|---|---|
| 34907A (Multifunction module) | |
| DAC range | ±12 V |
| DAC resolution | 16 bit ($^{24\,V}/_{2^{16}} = 366.21\,\mu V$ per bit) |
| DAC maximum current | 10 mA |
| 34901A (20 channel multiplexer) | |

**Table A.6:** Keysight 34972A some SCPI commands

| Description | Example command | Example return |
|---|---|---|
| Read current measurement | `READ?` | `+2.00200000E+01` (20.02 °C) |
| Set DAC voltage of ch 204 to 3.1 V | `SOUR:VOLT 3.1,(@204)` | |

## A.3 Oscilloscopes

### A.3.1 Tektronix MSO64

**Table A.7:** Tektronix MSO64 specifications

| Specification | Value |
|---|---|
| Bandwidth | 6 GHz |
| Sample rate | 25 GS/s |
| ADC resolution | 12 bit |
| DC gain accuracy (@ 50 Ω, >2 mV/div) | ±2 % |

**Table A.8:** Tektronix MSO64 some SCPI commands

| Description | Example command | Example return |
|---|---|---|
| Read mean of measurement 1 (current acq.) | `MEASUrement:MEAS1:RESUlts:CURR:MEAN?` | `3.0685821787408` |

## A.4 RF signal generator

### A.4.1 Rohde and Schwarz SMC100A

**Table A.9:** Rohde and Schwarz SMC100A specifications

| Specification | Value |
|---|---|
| Frequency range | 9 kHz to 3.2 GHz |
| Maximum power level | 17 dBm |
| SSB phase noise (@ 1 GHz, $f_o = 20$ kHz, $BW = 1$ Hz) | −111 dBc |
| Level error | <0.9 dB |

**Table A.10:** Rohde and Schwarz SMC100A some SCPI commands

| Description | Example command | Example return |
|---|---|---|
| Set RF power level to 10.5 dBm | `SOUR:POW 10.5` | |
| Set RF frequency to 3.1 GHz | `SOUR:FREQ:FIX 3.1e9` | |
| Enable the RF output | `OUTP on` | |

## A.5 RF power meter

### A.5.1 HP E4419B

**Table A.11:** HP E4419B specifications

| Specification | Value |
|---|---|
| Digits | 4 |
| Accuracy (abs. without power sensor) | ±0.02 dB |
| **Power probe: E4412A** | |
| Frequency range | 10 MHz to 18 GHz |
| Power range | −70 dBm to 20 dBm |

**Table A.12:** HP E4419B some SCPI commands

| Description | Example command | Example return |
|---|---|---|
| Measure power on input 1 | `MEAS1?` | `+2.89435802E+000` (2.894 dBm) |

## A.6 Vector Network Analyzer

### A.6.1 Agilent E5071C

**Table A.13:** Agilent E5071C specifications

| Specification | Value |
|---|---|
| Frequency range | 9 kHz to 8.5 GHz |

## A.7 Phase noise analyzer

### A.7.1 Holzworth HA7062C

**Table A.14:** Holzworth HA7062C specifications

| Specification | Value |
|---|---|
| DUT input frequency | 10 MHz to 6 GHz |
| Measurement bandwidth | 0.1 Hz to 40 MHz offsets |

# Bibliography


[1] F. Hinterberger, *Physik der Teilchenbeschleuniger und Ionenoptik mit durchgerechneten Beispielen und 99 Übungsaufgaben mit vollständigen Lösungen*. Berlin, Heidelberg, New York: Springer, 1997, ISBN: 9783540612384.

[2] T. Wangler, *RF linear accelerators*. Weinheim: Wiley-VCH, 2008, ISBN: 9783527623426.

[3] K. I. Park, *Fundamentals of Probability and Stochastic Processes with Applications to Communications*. Springer International Publishing, Dec. 4, 2017, 288 pp., ISBN: 3319680749.

[4] F. Puente León, *Messtechnik*. Springer-Verlag GmbH, 2019, ISBN: 3662597667.

[5] A. Lapidoth, *A Foundation in Digital Communication*. Cambridge University Press, Mar. 26, 2019, 920 pp., ISBN: 1107177324.

[6] P. Stoica, *Introduction to spectral analysis*. Upper Saddle River, N.J: Prentice Hall, 1997, ISBN: 0132584190.

[7] D. Rowell. (2008). "2.161 Signal Processing: Continuous and Discrete, Massachusetts Institute of Technology: MIT OpenCourseWare'', [Online]. Available: `https://ocw.mit.edu/courses/mechanical-engineering/2-161-signal-processing-continuous-and-discrete-fall-2008/#`.

[8] P. Welch, "The use of fast Fourier transform for the estimation of power spectra: A method based on time averaging over short, modified periodograms'', *IEEE Transactions on Audio and Electroacoustics*, vol. 15, no. 2, pp. 70–73, Jun. 1967. DOI: `10.1109/tau.1967.1161901`.

[9] L. R. Dalesio, M. R. Kraimer, and A. J. Kozubal, "EPICS Architecture'', *ICALEPCS*, vol. 91, 1991.

[10] Control System Studio. (2021). "Control System Studio'', [Online]. Available: `https://controlsystemstudio.org/about` (visited on 05/26/2021).

[11] M. Newville and A. Gratton. (2019). "PyEpics: Python Epics Channel Access'', [Online]. Available: `https://cars9.uchicago.edu/software/python/pyepics3/`.

[12] RadiaBeam, *Faraday Cups*. [Online]. Available: `http://www.radiabeam.com/upload/catalog/pdf/14272334342015-03-24_faraday-cups.pdf`.

[13] P. Synotech, *PCB 421A25 Charge Amplifier*.

[14] Mini-Circuits, *ZX73-2500+ Voltage Variable Attenuator*.

[15] R. W. Waugh, "A Low-Cost Surface Mount PIN Diode $\pi$ Attenuator'', vol. 35, no. 5, pp. 280–284, 1992.

[16] The LXI Consortium. (May 29, 2021). "LXI instrument communication'', [Online]. Available: `https://www.lxistandard.org/about/vxi-11-and-lxi.aspx`.